

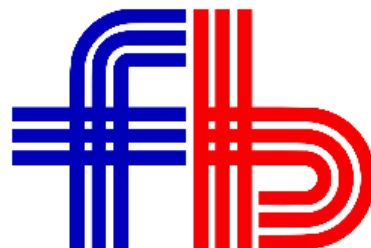


**Politecnico  
di Torino**

**Politecnico di Torino**

DEPARTMENT OF MECHANICAL AND AEROSPACE ENGINEERING (DIMEAS)  
Master's in Mechanical Engineering A.Y. 2024/2025  
April 2025

# **Modeling the dynamic behavior of two coupled parallel conductors**



Supervisors:

Prof. Dario Anastasio  
Eng. Mattia Passuello

Candidate:

Marco Costantini



## Abstract

Electric energy transport is receiving a big push in the last years due to the increase of consumption worldwide. Relatively to the high voltage overhead lines, completely new requirements for the conductors, fittings and damping devices have been defined with the scope of boosting the performance of the current net without changing the structures already built for the existing lines (i.e. the towers). The challenge is to enhance the existing lines by replacing the installed conductors with new ones, especially with new carbon fibre core conductors with very low SAG and increased capacity for the same diameter, together with the goal of evolving in a green way, fulfilling lower limits of CO<sub>2</sub> emission and lower EM noise requirements. For the involved companies, this challenge demands the research of new solutions starting from a deep review of the status of the art of the products to reach out their optimization. With this focus, the new designs need to be investigated from the fundamental equation in order to see if an improvement is possible and how to make it. The aim of the present thesis is exactly this: under the light of new techniques know in literature, do a review of the modal analysis of single and coupled conductors to compute the dynamical response of a vibrating span of the line. What above is of crucial importance for the optimisation of the dampers and spacer-dampers, and also to make a sensitivity analysis of the modal parameters involved in the phenomena to understand the fatigue process of the conductors.

The thesis is structured as follows.

Chapter 1 provides a general overview of the dynamic phenomena of the overhead lines.

In Chapter 2, the analysis starts with the modal analysis of the conductor basic model: the Euler-Bernoulli beam. The solution technique for a pinned-pinned E-B beam is shown: first, the equilibrium equation of the free body diagram of a beam element are written; then, trying a solution by separation of space and time variables, independent equations for space and time are found. After that, by imposing the boundary conditions, the eigenfunctions are computed together with the modal parameters. Finally, the solution of the equation is given by series representation.

Bearing in mind the obtained results, a more representative equation is studied: the taut Euler-Bernoulli beam. The boundary conditions are the same (pinned-pinned), but the addition of the tensioning term modifies the modal parameters. The eigenfunctions previously obtained are now used as a comparison function to obtain the modal parameters and solve the equation. The solution procedure is the same, and a new formula for the solution by series is found. This equation is the base for the coupled configuration.

Additionally, self-damping is taken in consideration. Based on a wide used model know in literature, a hysteretic damping coefficient per unit length is introduced, accounting this way a dissipative force into the equation of equilibrium. Using an experimentally determined hysteretic constant, the refined model improves the accuracy of cable vibration.

In Chapter 3, a distributed parameter model of two conductors is presented for the analysis of the coupled dynamics. The cables are modelled like taut Euler-Bernoulli beams while the loads

applied are modelled like distributed forces. The beams are linked by elastic spacers with lumped masses and stiffness equivalent to a real spacer-damper used for these conductors. The general solution is sought by the Ritz-Galerkin method, using a set of comparison function obtained in Chapter 2 for both the cables. After solving the eigen problem of the system, both the modal parameters and a time solution of the beams are derived.

In Chapter 4, the Matlab script is initially validated. To do so, the natural frequencies of the single cable obtained with the script are compared with the analytical ones and with the results know in literature for a specific case study. The script is run with different number of modes, in order to seek for the convergency of the solution both for the single conductor case and for the coupled conductors.

In Chapter 5, the modal shapes are shown and discussed in order to put in evidence subspan behaviour of the coupled motion. The time response of the system is checked at different points on the span trough a sensitivity analysis of the main parameters: number of spacer-dampers, their stiffness, external force amplitude, cable tensioning and self-damping are investigated for different magnitudes to see the effect on system output given the same input and verifying the very low sensitivity to cable self-damping.

Further analysis could be focused on the spacer-dampers damping effect, but they need a different representation due the out diagonal terms in the damping matrix. Another interesting development would be the study of conductors bundle as triple, quad, hexa etc. those are of current use in the overhead lines, together with the real wind excitation coming from lab tests. The distribution of the wind (i.e.the force) can be used to determine the real strain field on the conductors of the bundle, making possible a prediction of the fatigue behaviour and a life estimation of the line.



## Contents

1	Introduction .....	11
1.1	Excitation phenomena .....	11
1.2	Aeolian Vibration .....	12
1.3	Sub-span oscillation .....	13
2	Dynamical problem of a single conductor .....	15
2.1	The Euler-Bernoulli beam .....	16
2.1.1	Modal Parameters .....	18
2.2	Taut and forced Euler-Bernoulli beam .....	19
2.2.1	Modal Parameters .....	19
2.2.2	Time response for a generic forced case .....	20
2.3	Damped taut Euler-Bernoulli beam .....	22
2.3.1	Modal parameters .....	23
2.3.2	Time response in damped case .....	24
3	Dynamical problem of coupled conductors .....	25
3.1	Coupled conductors with self-damping.....	29
3.2	A real kind of links: spacer-dampers .....	29
3.3	Dynamical problem of coupled conductors with spacer-damper .....	31
4	Simulations.....	33
4.1	Script verification.....	33
4.2	Parameters .....	35
4.3	Number of modes.....	36
5	Results.....	37
5.1	Undamped conductors.....	37
5.1.1	Effect of the number of spacer-dampers .....	38
5.1.2	Variation of the spacer-damper stiffness $k_{AB}$ .....	43
5.1.3	Variation of the conductor pulling force $T$ .....	47
5.1.4	Variation of the external force magnitude $F_c$ .....	50
5.1.5	Variation of wind velocity $v$ .....	51
5.1.6	Variation of spacer damper mass $m_{AB}$ .....	54
5.2	Damped conductors.....	57
5.2.1	Effect of the self-damping coefficient on coupled cables .....	58

6 Conclusion .....	61
APPENDIX.....	62
Appendix A – Euler-Bernoulli beam.....	62
Appendix B – Eigenfunctions calculation.....	64
Appendix C – Modal equation of Euler-Bernoulli beam .....	66
Appendix D – Conductor self-damping term .....	67
Appendix E – Modal matrix calculation .....	69
Appendix F – Modal matrix of the coupled system.....	72
Bibliography.....	79

## List of figures

Figure 1: Analysis of Wind-Induced Vibrations on HVTL Conductors .....	11
Figure 2: Wind-induced phenomena and frequencies .....	12
Figure 3: Vortex Shedding .....	13
Figure 4: Typical subspan oscillation shape for a quad bundle .....	14
Figure 5: Euler-Bernoulli beam, pinned-pinned ends .....	16
Figure 6: Modal shapes of an E-B beam .....	18
Figure 7: Taut Euler-Bernoulli scheme .....	19
Figure 8: Displacement of a node at $L/4$ .....	21
Figure 9: Coupled conductors .....	25
Figure 10: Twin spacer-damper by Bertolotti .....	30
Figure 11: Spacer damper, Cinematic scheme .....	30
Figure 12: Spacer damper, Dynamic scheme .....	30
Figure 13: Coupled conductors with damping spacers .....	31
Figure 14: 1st, 2nd, 3rd, 4th ,5th, 50th and 100th modal shape .....	34
Figure 15: Cable structure, core + wires .....	35
Figure 16: Displacement comparison changing $N$ .....	36
Figure 17: System configuration .....	37
Figure 18: One spacer damper, first three modes .....	38
Figure 19: One spacer damper, middle modes .....	39
Figure 20: One spacer damper, last three modes .....	39
Figure 21: Two spacer-damper, first three modes .....	40
Figure 22: Two spacer-dampers, middle modes .....	40
Figure 23: Two spacer-dampers configuration, last three modes .....	41
Figure 24: Seven spacer-dampers, first three modes .....	41
Figure 25: Seven space-dampers, subspan modes .....	42
Figure 26: Seven space-dampers, last three modes .....	42
Figure 27: Rigid connection, node of joint and closer nodes .....	44
Figure 28: Rigid connection, random node .....	45
Figure 29: Spacer damper, node of joint .....	45
Figure 30: Spacer damper, nodes close to join and random node .....	46
Figure 31: Node of connection, 15%,20%,25% Tensioned .....	48

Figure 32: Midspan node, 15%,20%,25% Tensioned .....	49
Figure 33: Variation of force module .....	50
Figure 34: Variation of wind velocity, node of connection.....	52
Figure 34: Variation of wind velocity, midspan node.....	53
Figure 35: Variation of spacer's mass, node of connection .....	55
Figure 36: Variation of spacer's mass, midspan node .....	56
Figure 37: Displacements, undamped and with $H=1500$ .....	57
Figure 38: Displacement with different values of $H$ .....	58
Figure 39: Couple conductor displacement, undamped and $H=1500$ .....	59
Figure 40: Couple conductor displacement, $H=15000$ and $H=150000$ .....	60
Figure 41: Free-body diagram for a beam element .....	62

## List of Tables

Table 1: Damping coefficient for different modes .....	23
Table 2: Natural frequencies comparison .....	33
Table 3: Cable parameters.....	35

# 1 Introduction

Overhead power transmission lines are continuously exposed to environmental forces, among which wind-induced phenomena play a critical role in their structural behaviour and long-term reliability. Wind effects can cause various types of vibrations and oscillations in transmission line conductors, leading to mechanical fatigue, material degradation, and potential failures if not properly mitigated. The next session gives a brief overview of the most common wind-induced vibrations those occur on over-head line conductors.

## 1.1 Excitation phenomena

The main wind-induced problems that can be seen on overhead lines are:

- Aeolian Vibration
- Subspan oscillations
- Galloping

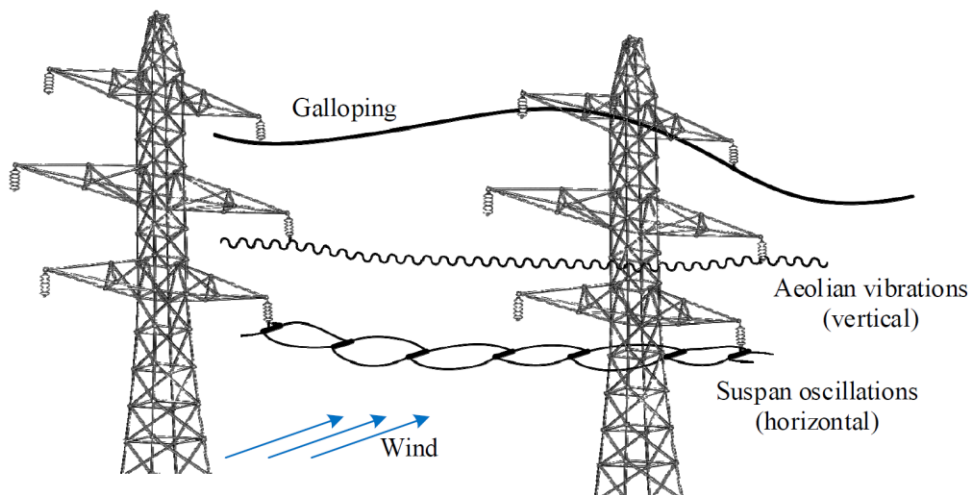


*Figure 1: Analysis of Wind-Induced Vibrations on HVTL Conductors*

Aeolian vibrations is the name associated to Vortex Induced Vibrations (VIV). They are due to vortex shedding from the conductors and can produce fatigue failures of the conductors themselves.

Subspan oscillations occur on conductor bundles and originate from wake produced by the windward conductor on the leeward one.

Galloping is a kind of instability due to the unstable shape assumed by the conductors when they are covered with ice.

As shown in Figure 2, aeolian vibrations occur for low to mean wind speeds – up to about 10m/s; subspan oscillations are excited by wind speeds in the range 8 ÷ 20 m/s and galloping generally occurs for high wind speeds, over 15 m/s.

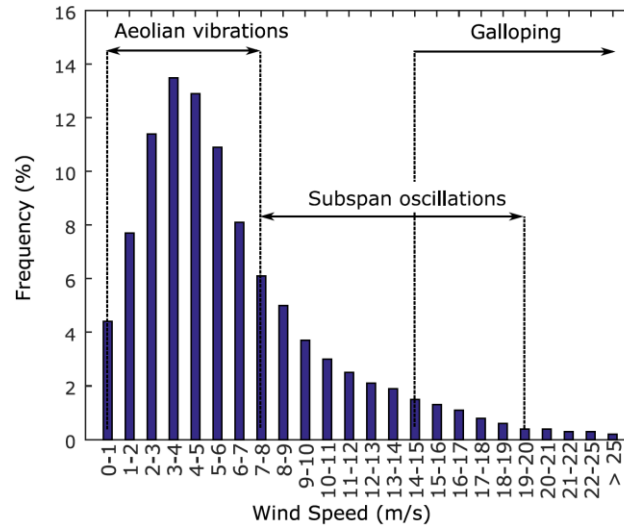


Figure 2: Wind-induced phenomena and frequencies

## 1.2 Aeolian Vibration

The main factors affecting aeolian vibrations are the span length, the tension and the type of terrain: is most severe when the conductor tension is high, the span is long and the terrain is smooth with low-to-moderate steady wind [1]. The roughness of the terrain determines the level of wind turbulence. Increasing the roughness of terrain, the turbulence level increases.

The vertical movements are associated to the vortex shedding phenomenon, where air currents over a cylindrical surface generate and release vortices. This leads to a periodic force on the body itself and if the associated frequency is close to of the body natural frequencies, the body starts to oscillate. The vortex shedding frequency is related to the body shape and dimensions, through the following formula:

$$f_s = St \frac{V}{D}$$

Where V is the speed of the flow, D is diameter and St is the Strouhal number that is related to the body shape. For a circular cylinder the Strouhal number St is 0,2.

$$St = \frac{f_s D}{V} = \frac{1}{V_r}$$

Where  $V_r$  is the reduced velocity.

Having the body natural frequency  $f_p$ , the critical velocity  $V_p$  at which the body will vibrate is:

$$V_p = \frac{f_p D}{St} = V_{St}$$

Also called Strouhal velocity.

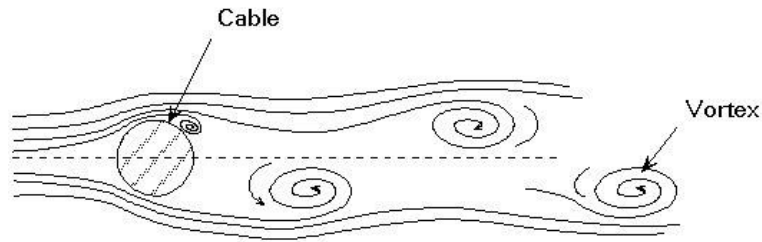


Figure 3: Vortex Shedding

The first natural frequency of a typical overhead transmission line conductor is of the order or 0.1 Hz. Therefore, the range of 10-50 Hz, over which aeolian vibration is generally analysed, approximately corresponds to the interval from the 100th to 500th eigenfrequencies of the cable. This means that almost certainly the vortex shedding frequency matches a natural frequency of the cable and transmission lines exposed to low to moderate wind are persistently subjected to aeolian vibration.

### 1.3 Sub-span oscillation

Subspan oscillations refer to localized vibrational modes that occur in structures with intermediate connections, such as conductors linked by spacers. These oscillations typically arise when the substructures between junction points experience dynamic coupling, leading to resonance phenomena at specific frequencies.

The oscillations are characterized by a frequency around 1 Hz, which corresponds to the mode of vibration of a section of conductor between two spacers [1].

Depending on the system properties, subspan oscillations can be either beneficial or detrimental: they may help dissipate energy in some cases but can become large enough to cause sub-conductors to collide.

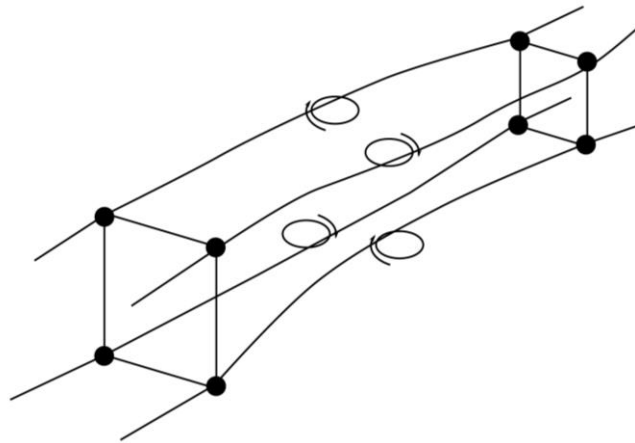


*Figure 4: Typical subspan oscillation shape for a quad bundle*

Additionally, these oscillations create strain on the sub-conductors at the spacer clamps and exert forces on the spacer arms, which may result in damage to the sub-conductor wires and loosening of the spacer clamps. Understanding the conditions that trigger these oscillations, as well as the role of damping, stiffness distribution, and coupling effects, is crucial for designing structures that remain stable under various loading conditions.

## 2 Dynamical problem of a single conductor

The easiest model to represent the dynamical behaviour of a conductor is to see it as a vibrating Euler-Bernoulli beam. The hypothesis of the study case are the usual ones:

- The static deformation, i.e. the catenary shape, does not enter the dynamic problem, so the beam is considered straight.
- The oscillation around the static position is small compared to the length, so the equations are linear, and the superposition principle applies.
- The beam position at rest is represented by its neutral axis, so all the displacements involved in the kinematic are independent from each other.
- Shear stress is neglected.
- Internal damping is absent.
- External excitation is absent.
- Mass and stiffness parameters are constant along the axis.

With this very well know model, given the boundary conditions (in our case pinned-pinned) one can compute the eigenfunction and estimate the modal parameters. If the initial conditions are given too, the dynamical problem can be completely solved in the form of infinite series, as explained in Appendix C.

A more representative model is the taut Euler-Bernoulli beam, that is the same described above but with an added term that depends on the tensioning. This term modifies the modal parameters and, especially, one can see that the natural frequencies become dominated by the tensioning term when it's large enough.

Internal damping can be added to the beam model using a hysteretic model for the forces. The model obtained with this last addition is the most used in literature (see [2] for reference), and the damping coefficient is computed among the other model parameters.

In the next paragraphs, the above models are developed. The focus is twofold: collecting the fundamental results of each model and showing the solution technique of the equations, useful to treat the kernel problem of the thesis, i.e., the coupled conductors.

## 2.1 The Euler-Bernoulli beam

The conductor could be represented through the model of a simply supported beam shown in Figure 5. In this scheme:

- Vertical displacement is  $w(x, t)$ .
- Bending stiffness of the cross-section  $EI$  is constant.
- Linear mass  $\mu$  is constant.

The Euler Bernoulli beam theory assumes that:

- Rotation is negligible compared to translation allowing neglect of rotational inertia effects.
- Angular distortion due to the shear is small in relation to the bending deformation.

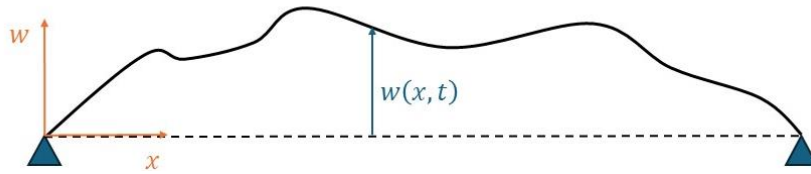


Figure 5: scheme of the Euler-Bernoulli beam with pinned-pinned ends

The equilibrium equation, obtained in Appendix A, is:

$$\mu \frac{\partial^2 w}{\partial t^2} + EI \frac{\partial^4 w}{\partial x^4} = 0 \quad (1)$$

The standard approach is to separate the variables:

$$w(x, t) = \Phi(x)\eta(t)$$

where  $\Phi(x)$  is the eigenfunction which represent the modal shape and is to be computed by imposing the boundary conditions,  $\eta(t)$  is the modal coordinate which represent how the amplitude of the shape varies with time. Modal coordinates are of the kind:

$$\eta(t) = A \cos(\omega t) + B \sin(\omega t)$$

To find out the solution, we specify the boundary condition at the ends. Being pinned ends, the deflection and slope of the bending moment are zero, so that the boundary conditions are:

$$w(0, t) = w(L, t) = 0 \quad \text{and} \quad \left. \frac{\partial w^2(x, t)}{\partial x^2} \right|_{x=0} = \left. \frac{\partial w^2(x, t)}{\partial x^2} \right|_{x=L} = 0 \quad (2)$$

Finally, we get infinite eigenfunctions (see Appendix B) of the kind:

$$\Phi_n(x) = \sin\left(\frac{n\pi x}{L}\right) \quad (3)$$

And the solution can be expressed in the form of series:

$$w(x, t) = \sum_{n=1}^{\infty} \Phi_n(x) \eta_n(t) \quad (4)$$

This formulation serves as the foundation for further analysis, including modal analysis and response to forced excitations. The eigenfunction of the pinned-pinned case will be used as comparison function to compute the modal parameters of all the other case treated in this thesis and for this reason it can be considered the fundamental expression obtained in this chapter.

## 2.1.1 Modal Parameters

By substituting  $w(x, t)$ , eq. (4), into the governing equation (1), integrating over the spatial domain and applying the orthogonality property of the eigenfunctions we obtain infinite modal equations (see Appendix C). For each mode  $n$ :

$$\frac{L}{2} \mu \ddot{\eta}_n + \frac{L}{2} \left( \frac{n\pi}{L} \right)^4 EI \eta_n = 0 \quad (5)$$

The modal parameters are defined as:

$$\begin{cases} m_n = \frac{L}{2} \mu \\ k_n = \frac{L}{2} \left( \frac{n\pi}{L} \right)^4 EI \\ \omega_n^2 = \frac{k_n}{m_n} = \left( \frac{n\pi}{L} \right)^4 \left( \frac{EI}{\mu} \right) \end{cases}$$

The first four modal shapes are represented in Figure 6.

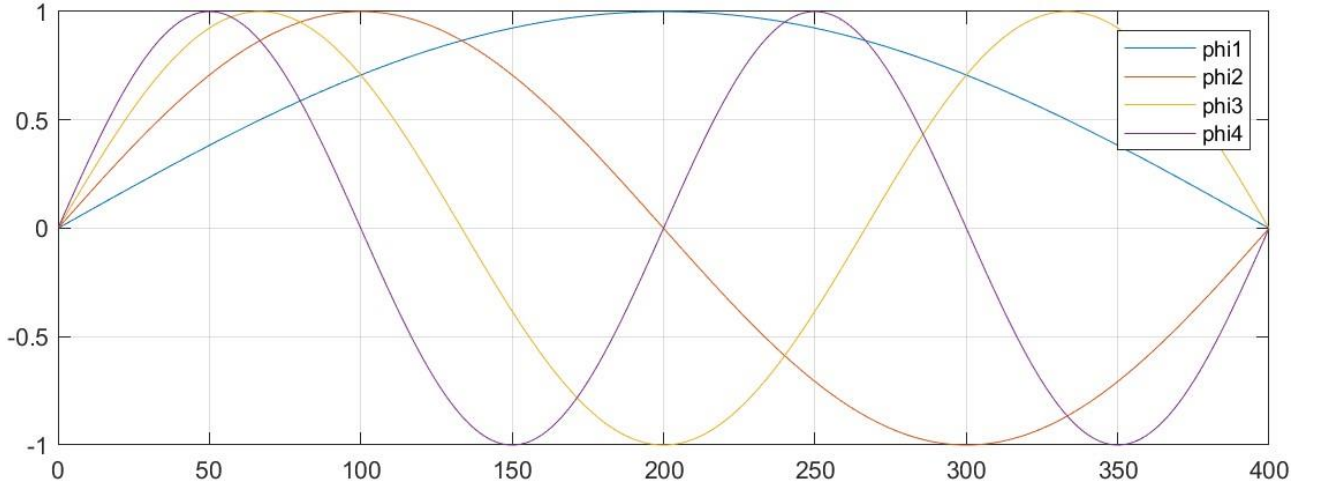


*Figure 6: Modal shapes of a pinned-pinned Euler-Bernoulli beam*

## 2.2 Taut and forced Euler-Bernoulli beam

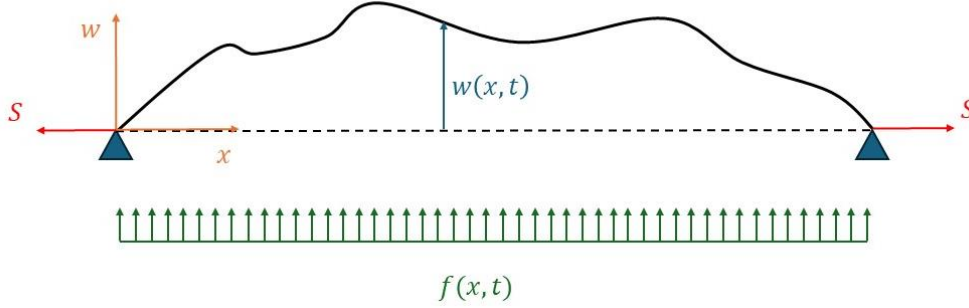


Figure 7: scheme of the taut Euler-Bernoulli beam with pinned-pinned ends

High voltage conductors are cables suspended between towers, experiencing a high axial tensile force due to their weight. To make the model more realistic, we modify the governing equation to include the effect of the axial tension:

$$\mu \frac{\partial^2 w}{\partial t^2} + EI \frac{\partial^4 w}{\partial x^4} - S \frac{\partial^2 w}{\partial x^2} = f(x, t)$$

where  $S \frac{\partial^2 w}{\partial x^2}$  is the additional term accounting for the axial tension  $S$  which is assumed constant,  $f(x, t)$  represents the force per unit length acting on the cable. This model better represents high-voltage conductors combining elements of a flexible beam (bending stiffness  $EI$ ) and a tensioned string (axial tension  $S$ ). The axial tension  $S$  is assumed to be positive in tension.

### 2.2.1 Modal Parameters

The addition of the tensioning term modifies the modal parameters. The eigenfunction (3) obtained previously is now used as a comparison function to obtain the modal parameters and solve the equation. The solution procedure is the same, we get infinite modal equations of the kind:

$$m_n \ddot{\eta}_n + k_n \eta_n = f_n \quad (6)$$

where the modal parameters are:

$$\left\{ \begin{array}{l} m_n = \frac{L}{2}\mu \\ k_n = \frac{L}{2}\left(\frac{n\pi}{L}\right)^2 \left( \left(\frac{n\pi}{L}\right)^2 EI + S \right) \\ \omega_n^2 = \frac{k_n}{m_n} = \left(\frac{n\pi}{L}\right)^2 \left( \frac{S}{\mu} + \left(\frac{n\pi}{L}\right)^2 \frac{EI}{\mu} \right) \\ f_n = \int_0^L f(x, t) \Phi_n(x) dx \end{array} \right.$$

This result highlights how  $S$  influences the vibration characteristics of the cable. When tension is dominant, the system behaves similarly to a taut string. When bending stiffness is significant, higher order modes are affected.

## 2.2.2 Time response for a generic forced case

The conductor is subjected to the wind action. So, in the second member of eq. (6) there is a force generated by the wind. To understand the system's dynamic, we choose a simplified sinusoidal form:

$$f(x, t) = F_c \sin(\Omega t)$$

Where  $\Omega$  represents the angular frequency of the wind and  $F_c$  its amplitude.

The force is applied as a distributed load along the length of conductor. To reach this solution we introduce a Heaviside function  $H(x)$  which has these characteristics:

$$H(x) = \begin{cases} 0, & x < 0 \text{ and } x > L \\ 1, & 0 \leq x \leq L \end{cases}$$

This function ensures that the wind force is applied only within the length of the cable. At this point, the right-side term of eq. (6) becomes:

$$\int_0^L f(x, t) \Phi_n(x) dx = \int_0^L F_c \sin(\Omega t) H(x) \Phi_n(x) dx = \int_0^L F_c \sin(\Omega t) \sin\left(\frac{n\pi x}{L}\right) dx$$

We can develop the full equation for each mode:

$$\frac{L}{2}\mu\ddot{\eta}_n + \frac{L}{2}\left(\frac{n\pi}{L}\right)^2 \left( \left(\frac{n\pi}{L}\right)^2 EI + T \right) \eta_n = \int_0^L F_c \sin(\Omega t) \sin\left(\frac{n\pi x}{L}\right) dx$$

$$\ddot{\eta}_n(t) + \omega_n^2 \eta_n(t) = Q_n(t)$$

Where  $Q_n(t)$  is the generalized force for the mode  $n$ :

$$Q_n(t) = \frac{1}{m_n} \int_0^L F_c \sin(\Omega t) \sin\left(\frac{n\pi x}{L}\right) dx$$

$$Q_n(t) = \frac{F_c L [1 - \cos(n\pi)]}{m_n n\pi} \sin(\Omega t) \quad (7)$$

Using the convolution integral [3], with zero initial condition we reach the solution:

$$\eta_n(t) = \frac{1}{\omega_n} \int_0^t Q_n(\tau) \sin(\omega_n(t - \tau)) d\tau = \frac{F_c L [1 - \cos(n\pi)]}{m_n n\pi} \frac{1}{\omega_n^2 - \Omega^2} \left( \sin\Omega t - \frac{\Omega}{\omega_n} \sin\omega_n t \right) \quad (8)$$

Finally, the total displacement of the conductor, considering contributions from all the modes, is given by:

$$w(x, t) = \sum_{n=1}^N \Phi_n(x) \eta_n(t) = F_c \sum_{n=1}^N \frac{1}{m_n} \sin\left(\frac{n\pi x}{L}\right) \frac{L(1 - \cos(n\pi))}{n\pi} \frac{1}{\omega_n^2 - \Omega^2} \left( \sin\Omega t - \frac{\Omega}{\omega_n} \sin\omega_n t \right) \quad (9)$$

The displacement of the node at a quarter of the span  $w\left(\frac{L}{4}, t\right)$ , as shown in Figure 8, shows the periodic general behaviour of the system output. At each peak there is a steady-state condition where the node oscillates between two values.

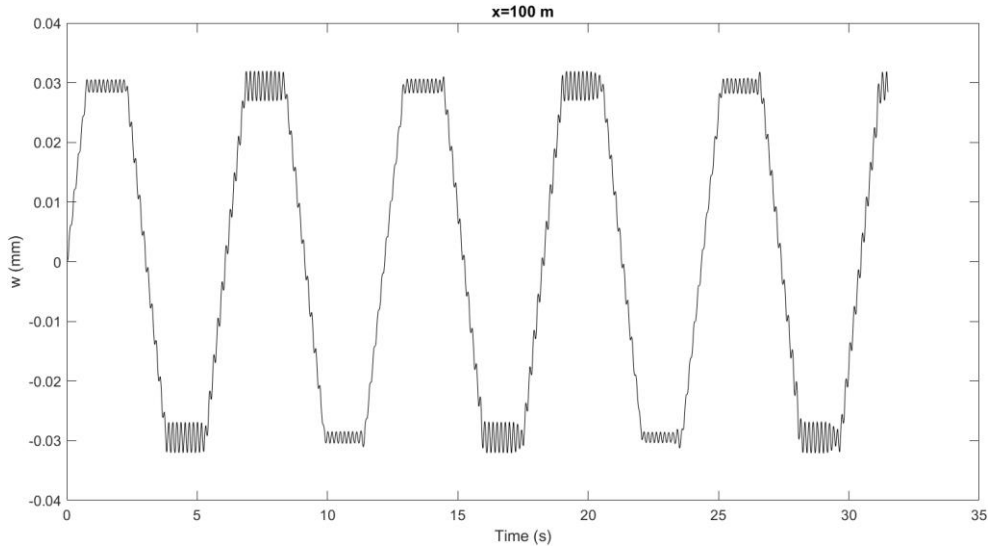


*Figure 8: Displacement of a node at L/4*

## 2.3 Damped taut Euler-Bernoulli beam

The system just analysed has the property of being able to vibrate freely with constant amplitude for an indefinite period because no dissipation of energy has been assumed. Studies conducted in the past [2] shows that the energy dissipated is directly proportional to the cable length. It is possible to assume a hysteretic damping coefficient for unit cable length that depends only on the cable structure and the vibration mode. A general damping force of this kind of system is given by:

$$F = h \frac{\dot{w}}{\Omega}$$

Where  $h$  is the hysteretic damping coefficient and  $\Omega$  is the angular frequency excited. In our case  $w(x, t) = \Phi(x)\eta(t)$ . Where  $\Phi(x)$  are the comparison functions  $\sin\left(\frac{n\pi x}{L}\right)$ .

Assuming that the energy dissipated by the conductor, vibrating in the  $n$ th mode, is due to unit damping forces distributed along the conductor and expressed by:

$$dF_n = \frac{h_n}{\Omega} \dot{\eta}_n \sin\left(\frac{n\pi x}{L}\right) dx$$

Where  $h_n$  is the dimensionless hysteretic damping coefficient for  $n$ th vibration mode. It depends linearly on the wavelength of each mode  $\lambda_n$  by this equation:

$$h_n = H\lambda_n^{-3}$$

$$\lambda_n = \frac{2L}{n}$$

$H$  represents the hysteretic constant of the cable. For a cable similar to ours (see [2]):

$$H = 1500.$$

Table 1 lists different values of hysteretic damping coefficient for different number of modes.

The total energy  $D$  dissipated during the motion of the conductor is the sum of the separate energies dissipated by each of the modes included in the solution:

$$D = \sum_n^N \frac{Lh_n}{4\Omega} \dot{\eta}_n^2(t)$$

Adding the energy dissipated to the equation of motion (see Appendix D) we obtain:

$$\frac{L}{2} \mu \ddot{\eta}_n + \frac{L}{2} \left(\frac{n\pi}{L}\right)^2 \left( \left(\frac{n\pi}{L}\right)^2 EI + S \right) \eta_n + \frac{Lh_n}{2\Omega} \dot{\eta}_n = \int_0^L f(x, t) \Phi_n(x) dx \quad (10)$$

*Table 1: Damping coefficients for different modes*

Mode number	$h_n$
1	$2.9 \times 10^{-6}$
2	$2.34 \times 10^{-5}$
5	$3.66 \times 10^{-4}$
10	0.0029
100	2.9
500	366
1000	$2.9 \times 10^3$

### 2.3.1 Modal parameters

By developing the previous eq. (10), we obtain:

$$m_n \ddot{\eta}_n + c_n \dot{\eta}_n + k_n \eta_n = f_n \quad (11)$$

The modal parameters result to be:

$$\left\{ \begin{array}{l} m_n = \frac{L}{2} \mu \\ k_n = \frac{L}{2} \left( \frac{n\pi}{L} \right)^2 \left( \left( \frac{n\pi}{L} \right)^2 EI + S \right) \\ \omega_n = \frac{n\pi}{L} \sqrt{\frac{S}{\mu} + \left( \frac{n\pi}{L} \right)^2 \frac{EI}{\mu}} \\ c_n = \frac{L h_n}{2\Omega} \\ f_n = \int_0^L f(x, t) \Phi_n(x) dx \end{array} \right.$$

Rearranging eq. (11), we get:

$$\ddot{\eta}_n(t) + \omega_n^2 \eta_n(t) + \frac{h_n}{2\Omega m_n} L \dot{\eta}_n = Q_n(t)$$

The hysteretic coefficient can be written as an equivalent viscous coefficient as:

$$\frac{h_n}{2\Omega m_n} L = 2\zeta_n \omega_n$$

$$\zeta_n = \frac{h_n}{4\Omega m_n \omega_n} L$$

where  $\zeta_n$  is the viscous damping ratio.

It is also possible to introduce the  $n$ th frequency of damped vibration, called  $\omega_{dn}$ :

$$\omega_{dn} = \omega_n \sqrt{1 - \zeta_n^2} = \omega_n \sqrt{1 - \left(\frac{h_n}{4\Omega m_n \omega_n} L\right)^2}$$

### 2.3.2 Time response in the damped case

The solution is given by the convolution integral:

$$\begin{aligned} \eta_n(t) &= \int_0^t \frac{1}{\omega_{dn}} Q_n(\tau) e^{-\zeta_n \omega_n (t-\tau)} \sin \omega_{dn} (t - \tau) d\tau \\ &= \frac{F_c}{m_n} \frac{L(1 - \cos(n\pi))}{n\pi} \frac{1}{\omega_{dn}^2 - \Omega^2} \left( \sin \Omega t - \frac{\Omega}{\omega_{dn}} \sin \omega_{dn} t \right) e^{-\zeta_n \omega_n t} \end{aligned}$$

In terms of physical displacements this yields:

$$\begin{aligned} w(x, t) &= \sum_n^N \Phi_n(x) \eta_n(t) = \\ F_c \sum_{n=1}^N \frac{1}{m_n} \sin\left(\frac{\pi n x}{L}\right) \frac{L(1 - \cos(n\pi))}{n\pi} \frac{1}{\omega_{dn}^2 - \Omega^2} \left( \sin \Omega t - \frac{\Omega}{\omega_{dn}} \sin \omega_{dn} t \right) e^{-\zeta_n \omega_n t} \end{aligned}$$

### 3 Dynamical problem of coupled conductors

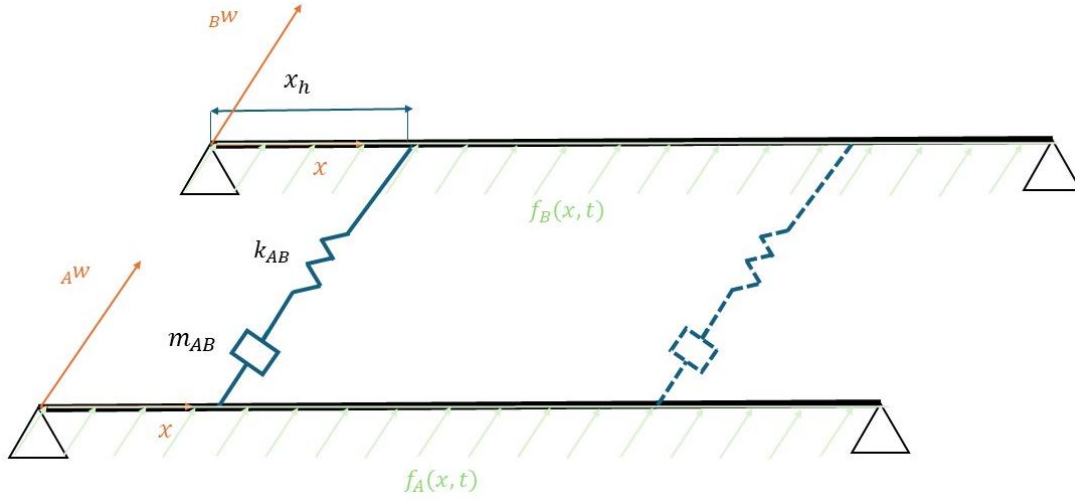


Figure 9: Coupled conductors

The model, shown in Figure 9, represents two parallel non damped pinned-pinned Euler-Bernoulli beams that are interconnected by a number  $H$  of elastic spacers with lumped masses and stiffness. These spacers introduce additional coupling between the beams, leading to two coupled equilibrium equations that govern the dynamic behaviour of the system.

The interaction between the beams is characterized by the elastic stiffness  $k_{AB}$  of the spacers and the presence of the equivalent mass of the spacer,  $m_{AB}$ . The contribution given by the spacer is mathematically described by a Dirac's delta function working only when  $x$  equals the position of the considered spacer  $x_h$ . This above-mentioned method is also adopted by Sorrentino et al. [4].

Let's label the two cables with the letters  $A$  and  $B$ . The two coupled equilibrium equations can be written in the form:

$$\begin{cases} \mu_A \frac{\partial^2 A_W}{\partial t^2} + k_A \frac{\partial^4 A_W}{\partial x^4} - S_A \frac{\partial^2 A_W}{\partial x^2} + \left( m_{AB} \frac{\partial^2 A_W}{\partial t^2} + k_{AB} (A_W - B_W) \right) \sum_{h=1}^H \delta(x - x_h) = f_A(x, t) \\ \mu_B \frac{\partial^2 B_W}{\partial t^2} + k_B \frac{\partial^4 B_W}{\partial x^4} - S_B \frac{\partial^2 B_W}{\partial x^2} + \left( m_{AB} \frac{\partial^2 B_W}{\partial t^2} + k_{AB} (B_W - A_W) \right) \sum_{h=1}^H \delta(x - x_h) = f_B(x, t) \end{cases} \quad (12)$$

Here  $\delta(*)$  is the Dirac distribution and  $f(x, t)$  represent the external force per unit length acting on the wire. In our case the two cables are identical so:

$$\begin{cases} \mu_A = \mu_B = \mu \\ k_A = k_B = k = EI \\ S_A = S_B = S \end{cases}$$

The solution is searched by the Ritz-Galerkin method, using the same set of  $N$  comparison function  $\{\Phi(x)\}$  to describe the two cables:

$$\begin{cases} {}_A W(x, t) = \{\Phi(x)\}^T \{{}_A \eta(t)\} \\ {}_B W(x, t) = \{\Phi(x)\}^T \{{}_B \eta(t)\} \end{cases} \quad (13)$$

$$\text{Where : } \{\Phi(x)\}_{N \times 1} = \begin{Bmatrix} \sin\left(\frac{\pi x}{L}\right) \\ \sin\left(\frac{2\pi x}{L}\right) \\ \vdots \\ \sin\left(\frac{N\pi x}{L}\right) \end{Bmatrix} \quad \{\eta(t)\}_{2N \times 1} = \begin{Bmatrix} \{{}_A \eta\}_{N \times 1} \\ \{{}_B \eta\}_{N \times 1} \end{Bmatrix}$$

After substituting the expression of  ${}_A W$  and  ${}_B W$  defined in eq. (13) in the equilibrium equation (eq. (12)), the latter are multiplied by  $\{\Phi(x)\}$  and integrated over the spatial domain. We get (see Appendix E for further details):

$$\begin{cases} \mu \frac{L}{2} [I] \{{}_A \ddot{\eta}\} + k \frac{L}{2} \text{diag}\left(\left(\frac{n\pi}{L}\right)^4\right) \{{}_A \eta\} + S \frac{L}{2} \text{diag}\left(\left(\frac{n\pi}{L}\right)^2\right) \{{}_A \eta\} + m_{AB} [\Sigma_h] \{{}_A \ddot{\eta}\} + k_{AB} [\Sigma_h] (\{{}_A \eta\} - \{{}_B \eta\}) = \\ \int_0^L \{\Phi(x)\} {}_A f(x, t) dx \\ \mu \frac{L}{2} [I] \{{}_B \ddot{\eta}\} + k \frac{L}{2} \text{diag}\left(\left(\frac{n\pi}{L}\right)^4\right) \{{}_B \eta\} + S \frac{L}{2} \text{diag}\left(\left(\frac{n\pi}{L}\right)^2\right) \{{}_B \eta\} + m_{AB} [\Sigma_h] \{{}_B \ddot{\eta}\} + k_{AB} [\Sigma_h] (\{{}_B \eta\} - \{{}_A \eta\}) = \\ \int_0^L \{\Phi(x)\} {}_B f(x, t) dx \end{cases}$$

These equations can be written in a matrix formulation by defining the following mass matrix  $M$  and stiffness matrix  $K$ :

$$\begin{aligned} [M]_{2N \times 2N} &= \frac{L}{2} \mu \begin{bmatrix} [I] & [0] \\ [0] & [I] \end{bmatrix} + m_{12} \begin{bmatrix} [\Sigma_h] & [0] \\ [0] & [\Sigma_h] \end{bmatrix} \\ [K]_{2N \times 2N} &= \frac{L}{2} \begin{bmatrix} [D] & [0] \\ [0] & [D] \end{bmatrix} + k_{12} \begin{bmatrix} [\Sigma_h] & -[\Sigma_h] \\ -[\Sigma_h] & [\Sigma_h] \end{bmatrix} \end{aligned}$$

The inner matrices are:

$$\begin{aligned} [I]_{N \times N} &= \text{diag}\{1\} \\ [\Sigma_h]_{N \times N} &= \sum_{h=1}^H \{\Phi(x_h)\} \{\Phi(x_h)\}^T \\ [D]_{N \times N} &= \text{diag}\left(\left(\frac{n\pi}{L}\right)^2 \left(\left(\frac{n\pi}{L}\right)^2 EI + T\right)\right) \end{aligned}$$

The systems of equations in terms of the mass and stiffness matrices are therefore:

$$[M]\{\ddot{\eta}\} + [K]\{\eta\} = \{F\} \quad (14)$$

As usual, we search the sets of eigenvalues and eigenfunctions by solving the undamped eigenproblem:

$$([K] - \omega_n^2[M])[Z] = 0$$

We get the modal matrix  $[Z]$ :

$$[Z]_{2N \times 2N} = \begin{bmatrix} [AZ] \\ [BZ] \end{bmatrix} = \begin{bmatrix} AZ_{1,1} & AZ_{1,2} & \dots & AZ_{1,2N} \\ AZ_{2,1} & AZ_{2,2} & \dots & AZ_{2,2N} \\ \vdots & \vdots & \ddots & \vdots \\ AZ_{N,1} & AZ_{N,2} & \dots & AZ_{N,2N} \\ BZ_{1,1} & BZ_{1,2} & \dots & BZ_{1,2N} \\ BZ_{2,1} & BZ_{2,2} & \dots & BZ_{2,2N} \\ \vdots & \vdots & \ddots & \vdots \\ BZ_{N,1} & BZ_{N,2} & \dots & BZ_{N,2N} \end{bmatrix}$$

$$\{\omega_n\} = \begin{Bmatrix} \omega_1 \\ \omega_2 \\ \vdots \\ \omega_{2N} \end{Bmatrix}$$

We can write:  $\{\eta(t)\} = [Z]\{p(t)\}$ , where  $\{p(t)\}$  is the vector of modal coordinates of the coupled system.

$$\{p(t)\}_{2N \times 1} = \begin{Bmatrix} p_1 \\ p_2 \\ \vdots \\ p_{2N} \end{Bmatrix}$$

Considering the cable A, its displacement field can be obtained by:

$${}_A w(x, t) = \{\Phi(x)\}^T \{ {}_A \eta(t) \} = \{\Phi(x)\}^T [AZ] \{p(t)\} = \{ {}_A \Psi(x) \}^T \{p(t)\}$$

Where  $\{ {}_A \Psi(x) \}$  represent the vector of modal shapes of size  $1 \times 2N$ . Thus, substituting and multiplying by  $[Z]^T$  the problem can be written as:

$$[Z]^T [M] [Z] \{\ddot{p}\} + [Z]^T [K] [Z] \{p\} = [Z]^T \{F\}$$

Giving:

$$[m_n] \{\ddot{p}\} + [k_n] \{p\} = [f_n]$$

All the matrices are diagonal, and we get the following modal parameters:

$$\left\{ \begin{array}{l} [m_n] = [Z]^T [M] [Z] = \begin{bmatrix} m_1 & 0 & 0 \\ 0 & \ddots & 0 \\ 0 & 0 & m_{2N} \end{bmatrix} \\ [k_n] = [Z]^T [K] [Z] = \begin{bmatrix} k_1 & 0 & 0 \\ 0 & \ddots & 0 \\ 0 & 0 & k_{2N} \end{bmatrix} \\ \omega_n^2 = \frac{k_n}{m_n} \\ [f_n] = [Z]^T \{F\} \end{array} \right.$$

so, we can write the equation for each mode (considering the force acting only on cable A):

$$\ddot{p}_n + \omega_n^2 p_n = \frac{F_c}{m_n} \sum_{r=1}^N {}_A Z_{r,n} \frac{L(1 - \cos(r\pi))}{r\pi} \sin(\Omega t)$$

After solving the convolution integral:

$$p_n(t) = \frac{F_c}{m_n} \left[ \sum_{r=1}^N {}_A Z_{r,n} \frac{L(1 - \cos(r\pi))}{r\pi} \right] \frac{1}{\omega_n^2 - \Omega^2} \left( \sin \Omega t - \frac{\Omega}{\omega_n} \sin \omega_n t \right)$$

Now we have all the variables to solve the problem:

$$\left\{ \begin{array}{l} \{\eta(t)\} = \begin{bmatrix} [{}_A Z] \\ [{}_B Z] \end{bmatrix} \{p(t)\} = \begin{Bmatrix} \{{}_A \eta\} \\ \{{}_B \eta\} \end{Bmatrix} \\ {}_A W(x, t) = \{\Phi(x)\}^T \{{}_A \eta(t)\} \\ {}_B W(x, t) = \{\Phi(x)\}^T \{{}_B \eta(t)\} \end{array} \right.$$

Substituting and solving we get the following solutions (detailed in Appendix F), considering the force acting only on cable A:

$$\left\{ \begin{array}{l} {}_A W(x, t) = \sum_{k=1}^N \sin\left(\frac{k\pi x}{L}\right) \left[ \sum_{n=1}^{2N} {}_A Z_{k,n} \frac{F_c}{m_n} \left( \sum_{r=1}^N {}_A Z_{r,n} \frac{L(1 - \cos(r\pi))}{r\pi} \right) \frac{1}{\omega_n^2 - \Omega^2} \left( \sin \Omega t - \frac{\Omega}{\omega_n} \sin \omega_n t \right) \right] \\ {}_B W(x, t) = \sum_{k=1}^N \sin\left(\frac{k\pi x}{L}\right) \left[ \sum_{n=1}^{2N} {}_B Z_{k,n} \frac{F_c}{m_n} \left( \sum_{r=1}^N {}_A Z_{r,n} \frac{L(1 - \cos(r\pi))}{r\pi} \right) \frac{1}{\omega_n^2 - \Omega^2} \left( \sin \Omega t - \frac{\Omega}{\omega_n} \sin \omega_n t \right) \right] \end{array} \right. \quad (15)$$

In case of force acting on both cables, the solution becomes:

$$\left\{ \begin{array}{l} {}_A W(x, t) = \sum_{k=1}^N \sin\left(\frac{k\pi x}{L}\right) \left[ \sum_{n=1}^{2N} {}_A Z_{k,n} \frac{F_c}{m_n} \left( \sum_{r=1}^N ({}_A Z_{r,n} + {}_B Z_{r,n}) \frac{L(1 - \cos(r\pi))}{r\pi} \right) \frac{1}{\omega_n^2 - \Omega^2} \left( \sin \Omega t - \frac{\Omega}{\omega_n} \sin \omega_n t \right) \right] \\ {}_B W(x, t) = \sum_{k=1}^N \sin\left(\frac{k\pi x}{L}\right) \left[ \sum_{n=1}^{2N} {}_B Z_{k,n} \frac{F_c}{m_n} \left( \sum_{r=1}^N ({}_A Z_{r,n} + {}_B Z_{r,n}) \frac{L(1 - \cos(r\pi))}{r\pi} \right) \frac{1}{\omega_n^2 - \Omega^2} \left( \sin \Omega t - \frac{\Omega}{\omega_n} \sin \omega_n t \right) \right] \end{array} \right.$$

In case of different forces with different angular frequencies  ${}_A \Omega \neq {}_B \Omega$ :

$$\begin{cases} {}_A W(x, t) = \sum_{k=1}^N \sin\left(\frac{k\pi x}{L}\right) \left[ \sum_{n=1}^{2N} {}_A Z_{k,n} \frac{1}{m_n} \left[ \sum_{r=1}^N {}_A Z_{r,n} {}_A F_c \frac{L(1-\cos(r\pi))}{r\pi} \sin({}_A \Omega t) + \sum_{r=1}^N {}_B Z_{r,n} {}_B F_c \frac{L(1-\cos(r\pi))}{r\pi} \sin({}_B \Omega t) \right] \frac{1}{\omega_n^2 - {}_A \Omega^2} \left( \sin({}_A \Omega t) - \frac{{}_A \Omega}{\omega_n} \sin \omega_n t \right) \right] \\ {}_B W(x, t) = \sum_{k=1}^N \sin\left(\frac{k\pi x}{L}\right) \left[ \sum_{n=1}^{2N} {}_B Z_{k,n} \frac{1}{m_n} \left[ \sum_{r=1}^N {}_A Z_{r,n} {}_A F_c \frac{L(1-\cos(r\pi))}{r\pi} \sin({}_A \Omega t) + \sum_{r=1}^N {}_B Z_{r,n} {}_B F_c \frac{L(1-\cos(r\pi))}{r\pi} \sin({}_B \Omega t) \right] \frac{1}{\omega_n^2 - {}_B \Omega^2} \left( \sin({}_B \Omega t) - \frac{{}_B \Omega}{\omega_n} \sin \omega_n t \right) \right] \end{cases}$$

### 3.1 Coupled conductors with self-damping

The system is the same of the undamped case (14), with the addition of the self-damping matrix  $[C]$ :

$$[M]\{\ddot{\eta}\} + [K]\{\eta\} + [C]\{\dot{\eta}\} = \{F\}$$

$$[C]_{2N \times 2N} = \frac{L}{2\Omega} \begin{bmatrix} [h] & 0 \\ 0 & [h] \end{bmatrix}$$

Where  $[h]_{N \times N} = \text{diag} \begin{pmatrix} h_1 \\ h_2 \\ \vdots \\ h_N \end{pmatrix}$  are the hysteretic self-damping constant of the cable for each mode.

Using the same procedure applied in 2.3.2 for single cable, we get the displacement formula. In case of force acting only on cable A:

$$\begin{cases} {}_A W(x, t) = \sum_{k=1}^N \sin\left(\frac{k\pi x}{L}\right) \left[ \sum_{n=1}^{2N} {}_A Z_{k,n} \frac{F_c}{m_n} \left( \sum_{r=1}^N {}_A Z_{r,n} \frac{L(1-\cos(r\pi))}{r\pi} \right) \frac{1}{\omega_{dn}^2 - \Omega^2} \left( \sin \Omega t - \frac{\Omega}{\omega_{dn}} \sin \omega_{dn} t \right) e^{-\zeta_n \omega_{dn} t} \right] \\ {}_B W(x, t) = \sum_{k=1}^N \sin\left(\frac{k\pi x}{L}\right) \left[ \sum_{n=1}^{2N} {}_B Z_{k,n} \frac{F_c}{m_n} \left( \sum_{r=1}^N {}_A Z_{r,n} \frac{L(1-\cos(r\pi))}{r\pi} \right) \frac{1}{\omega_{dn}^2 - \Omega^2} \left( \sin \Omega t - \frac{\Omega}{\omega_{dn}} \sin \omega_{dn} t \right) e^{-\zeta_n \omega_{dn} t} \right] \end{cases}$$

The only difference from undamped solutions (eq.(15)) is given by the multiplication term  $e^{-\zeta_n \omega_{dn} t}$  and by the substitution of  $\omega_n$  with  $\omega_{dn}$ .

### 3.2 A real kind of links: spacer-dampers

The basic design of a space-damper consists of a rigid frame on which two or more arms are connected by means of a rubber bushing through a shaft. Figure 10 shows the spacer-damper produced by Bertolotti:



*Figure 10: Twin spacer-damper by Bertolotti*

Wind force makes the cables move horizontally. In this way the spacer's arms rotate relatively to the body. The rotation is controlled by a certain stiffness of the hinge. Through some tests made by Bertolotti, which calculate the energy dissipated over a cycle, we can reach the value of the torsional stiffness.

Initially, we study the cinematic of the arm, showed in Figure 11.

$$\begin{cases} \delta w = b \delta\beta \sin(\beta + \delta\beta) \\ \delta u = \frac{\delta w}{\text{tg}(\beta + \delta\beta)} = b \delta\beta \cos(\beta + \delta\beta) \end{cases} \quad (16)$$

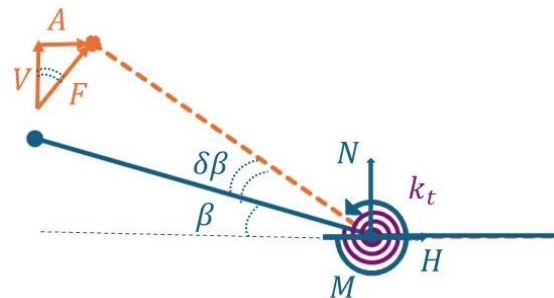
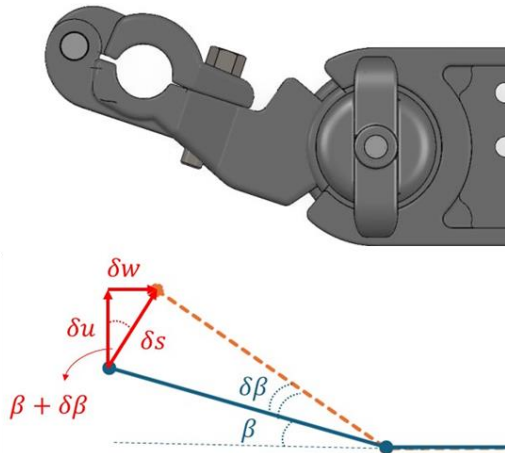


*Figure 11: spacer-damper, kinematic scheme*

*Figure 12: spacer-damper, dynamic scheme*

However, our primary interest is in the horizontal component of this force, which is responsible for damping the motion. The horizontal force  $A$  is given by:

$$A = F \sin(\beta + \delta\beta) = \frac{k_t \delta\beta}{b} F \sin(\beta + \delta\beta)$$

Comparing the last expression with the one of eq. (16) we get:

$$A = \frac{k_t}{b^2} \delta w = k_{AB} \delta w$$

Where  $k_{AB}$  is axial stiffness in the plane of the conductors.

This stiffness represents the effective stiffness of the spacer damper in resisting horizontal motion due to the applied forces and mitigates unwanted vibrations or resonances that could occur in the system.

The damping component  $c_{AB}$  is assumed to be proportional to  $k_{AB}$ .

### 3.3 Dynamical problem of coupled conductors with spacer-dampers

The model, shown in Figure 13, represents two parallel pinned-pinned Euler-Bernoulli beams with self-damping that are interconnected by H spacer-dampers with lumped masses.

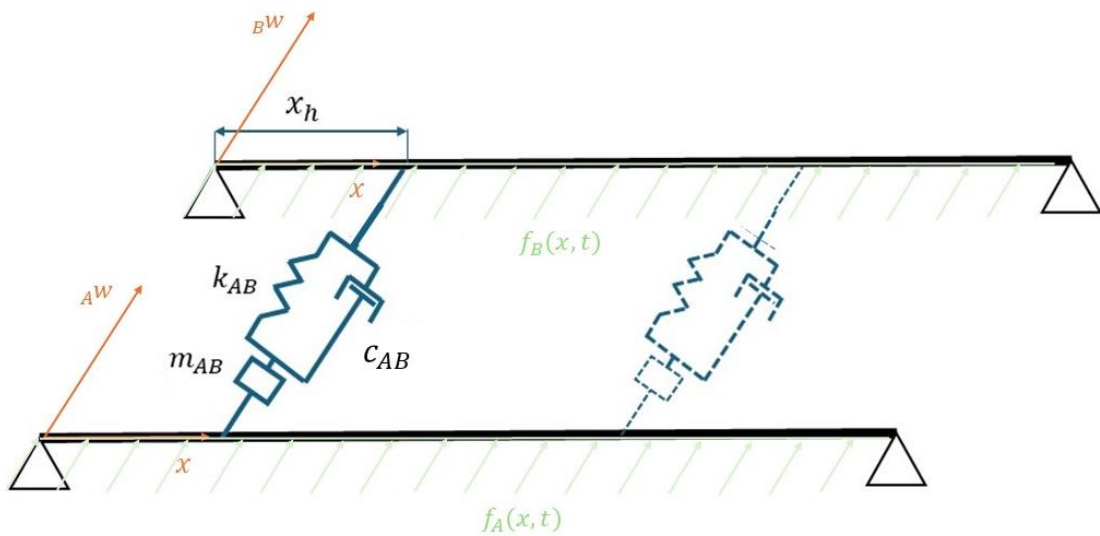


Figure 13: Coupled conductors with damping spacers

Considering only first cable (A), the following equation of motion holds:

$$\begin{aligned} \mu \frac{\partial^2 {}_A W}{\partial t^2} + k \frac{\partial^4 {}_A W}{\partial x^4} - S \frac{\partial^2 {}_A W}{\partial x^2} \\ + \left( m_{AB} \frac{\partial^2 {}_A W}{\partial t^2} + k_{AB} ({}_A W - {}_B W) + c_{AB} ({}_A \dot{W} - {}_B \dot{W}) \right) \sum_{h=1}^H \delta(x - x_h) \\ = {}_A f(x, t) \end{aligned}$$

Following the calculations of undamped case we get:

$$\begin{aligned} \mu \frac{L}{2} [I] \{ {}_A \ddot{\eta}(t) \} + k \frac{L}{2} \text{diag} \left( \left( \frac{n\pi}{L} \right)^4 \right) \{ {}_A \eta(t) \} + S \frac{L}{2} \text{diag} \left( \left( \frac{n\pi}{L} \right)^2 \right) \{ {}_A \eta(t) \} + m_{12} [\Sigma_h] \{ {}_A \ddot{\eta}(t) \} \\ + k_{AB} [\Sigma_h] (\{ {}_A \eta(t) \} - \{ {}_B \eta(t) \}) + c_{AB} [\Sigma_h] (\{ {}_A \dot{\eta}(t) \} - \{ {}_B \dot{\eta}(t) \}) \\ = \int_0^L \{ \Phi(x) \} {}_A f(x, t) dx \end{aligned}$$

$$[M] \{ \ddot{\eta} \} + [K] \{ \eta \} + [C] \{ \dot{\eta} \} = \{ F \}$$

Where  $[C]$ :

$$[C]_{2N \times 2N} = \frac{L}{2\Omega} \begin{bmatrix} [h] & 0 \\ 0 & [h] \end{bmatrix} + c_{AB} \begin{bmatrix} [\Sigma_h] & -[\Sigma_h] \\ -[\Sigma_h] & [\Sigma_h] \end{bmatrix}$$

Here, first matrix is related to the self-damping and second one to the damping induced by the spacers.

The system becomes non-diagonal and solving it would require further study using methods like Duncan's analysis. The displacement results can be obtained, but a more detailed acceptance calculation would be needed to fully quantify the effects, although this is outside the scope of this thesis.

## 4 Simulations

All the equations shown in the former paragraphs have been implemented on Matlab to check numerical results.

A first dutiful and rigorous check is done for a single cable in the case of a Euler-Bernoulli beam. The results for this simple case are well known in literature and a comparison with the analytical formula is easy to do. The focus is on the natural frequencies of the system those must turn out to be exact with an arbitrary number of digits.

Then the convergence of the solution for the coupled case obtained thanks to the Ritz-Galerkin method is verified. Since this is an approximated solution, the aim is to find the number  $N$  of comparison functions that gives a correct (negligible error) representation of the system response.

### 4.1 Script verification

Let us first consider a single undamped conductor. The natural frequencies calculated using analytical expressions are compared to results from the eigenvalue problem of eq. (5) developed with a Matlab script. The comparison is further extended to a previous study made by Gazzola [5]. Results are shown in Table 2.

*Table 2: Natural frequencies comparison*

Mode number	Analytical (Hz)	Script (Hz)	Gazzola (Hz)
1	0.1642	0.1642	0.1642
2	0.3284	0.3284	0.3284
3	0.4926	0.4926	0.4926
10	0.6569	0.6569	0.6569
50	0.8211	0.8211	0.8211
200	8.2720	8.2720	8.2720
500	129.9153	129.9153	129.9153

The modal shapes of the first 5 modes along with mode 50 and mode 100, evaluated by the numerical model are shown in Figure 14. These results demonstrate the potential of the proposed model in analysing the dynamic behaviour of the system.

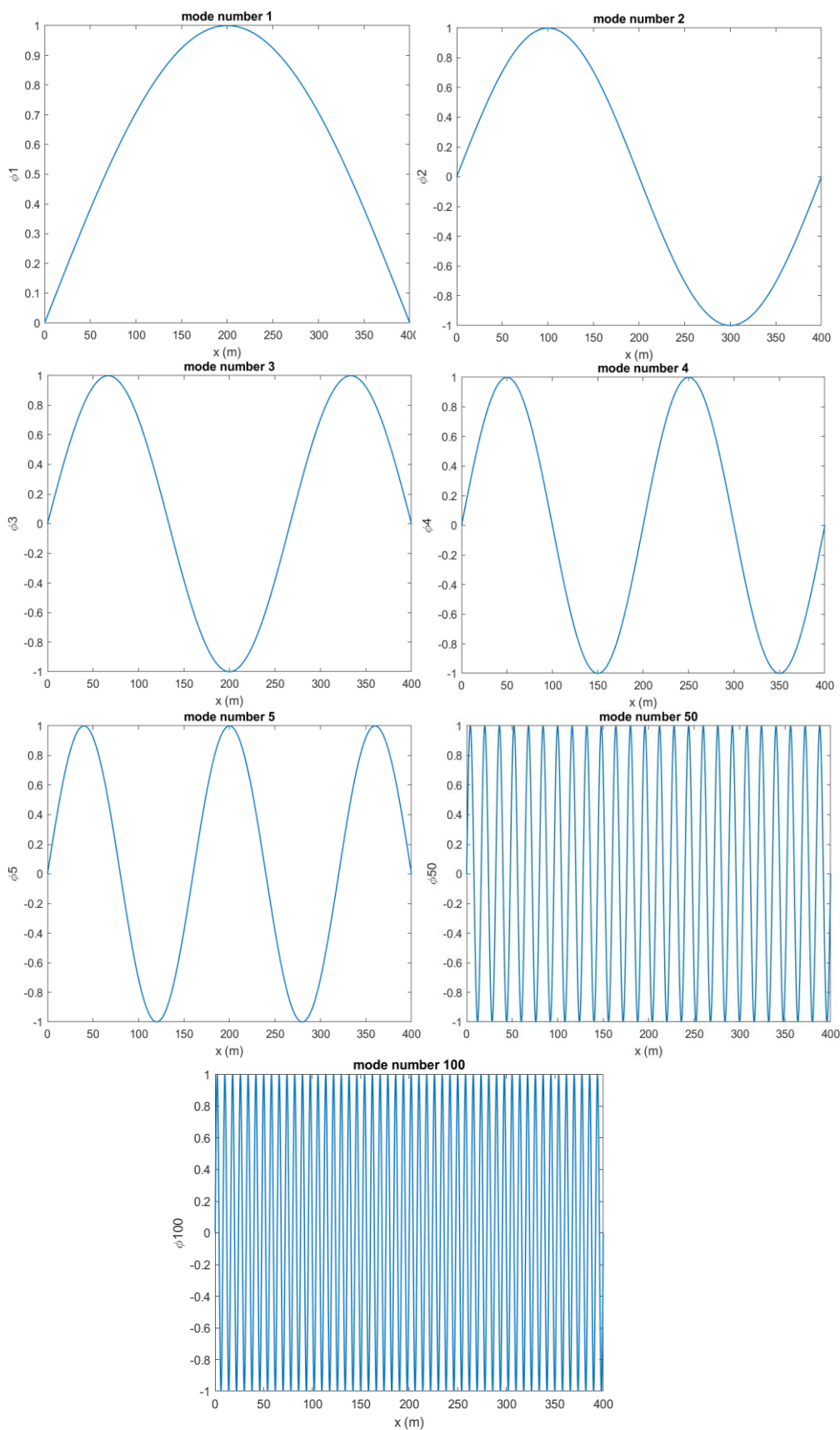


Figure 14: 1st, 2nd, 3rd, 4th, 5th, 50th and 100th modal shape

## 4.2 Parameters

Conductors are stranded cables. The most widely used form of conductors is that of layers of round wires stranded, first, around a so-called core, which can be of the same material or different, and then around each other. In our case the conductor is a core of steel surrounded by aluminium wires.

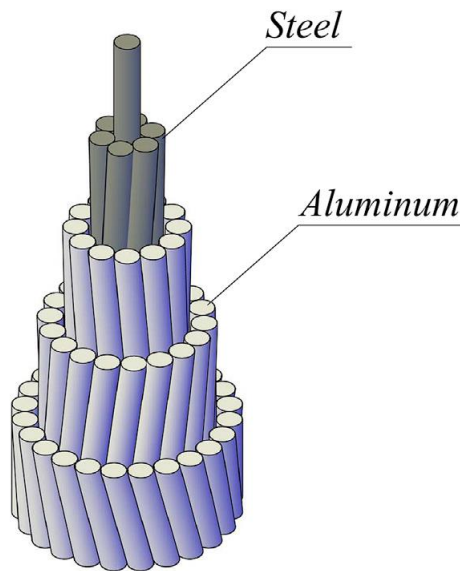


Figure 15: Cable structure, core + wires

Table 3: Cable parameters

Cable Property		Measurement unit
Length <b>L</b>	400	m
Diameter <b>D</b>	31.5	mm
Linear density <b><math>\mu</math></b>	1.953	kg/m
Young modulus <b>E</b>	68900	MPa
Flexural stiffness <b>EI</b>	3286	Nm <sup>2</sup>
Load braker <b>RTS</b>	168520	N
Tension <b>T</b> (20% RTS)	33704	N

### 4.3 Number of modes

Number of modes is an important parameter to choose. More modes improve accuracy but increase computational complexity. We need to include modes until the solution converges to a satisfactory accuracy. At least, modes included in the solution must describe the dynamical behaviour of the system nicely until the frequency of excitation of the wind  $f_{wind}$ . In order to get a better accuracy, we decide to set the frequency limit to:

$$f_{lim} = 1,2f_{wind}$$

And the corresponding limit number of modes is  $N_{lim}$ .

We compute the solution (described as a sum of modes) for increasing values of number  $N$  and see how the displacement  $w(x, t)$  varies.

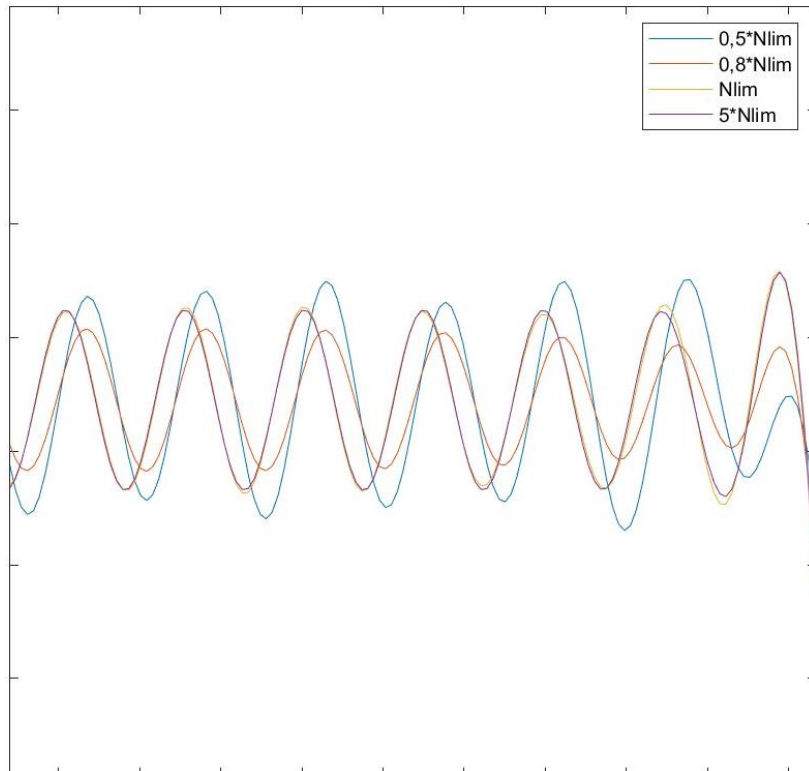


*Figure 16: Displacement comparison changing  $N$*

Figure 16 shows how the displacement  $w(x, t)$  changes as we increase the number of modes  $N$ . It shows that the displacement obtained with  $N_{lim}$  follows almost exactly the solution obtained with five times more modes. So, the previous choice of  $f_{lim}$  is a good truncation frequency. Therefore, it is unnecessary to use more modes beyond  $N_{lim}$ , which gives a good balance between computational efficiency and solution accuracy.

## 5 Results

In this study, we perform MATLAB simulations to analyse the behaviour of coupled conductors. The numerical simulations allow us to investigate key results such as modal shapes and time responses. By varying multiple parameters we get different results, providing valuable insights into the stability and vibration characteristics of the system.

The chapter is divided in 2 parts: first there is an analysis of the undamped coupled conductors case; then, the results of damped case.

### 5.1 Undamped conductors

The configuration selected for this section is shown in Figure 17, and represents two coupled conductors with one spacer placed at 52 m. The cable A is undergoing a distributed external force, given by a wind of velocity  $v = 1 \text{ m/s}$ .

Several cases will be analysed in this section, by varying the most important parameters of the system.

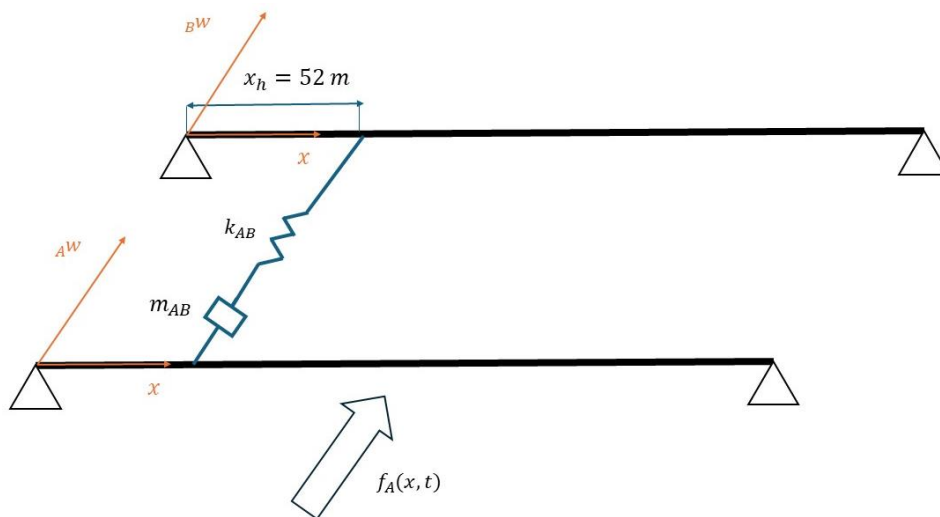


Figure 17: System configuration

## 5.1.1 Effect of the number of spacer-dampers

This subsection discussed the effects of the spacer dampers on the mode shapes of the coupled system. Cases with different positioning of spacer dampers are analysed.

- One spacer-damper

A single rigid spacer is considered. The first three modes are showed below. The second mode shows already the subspan behaviour.

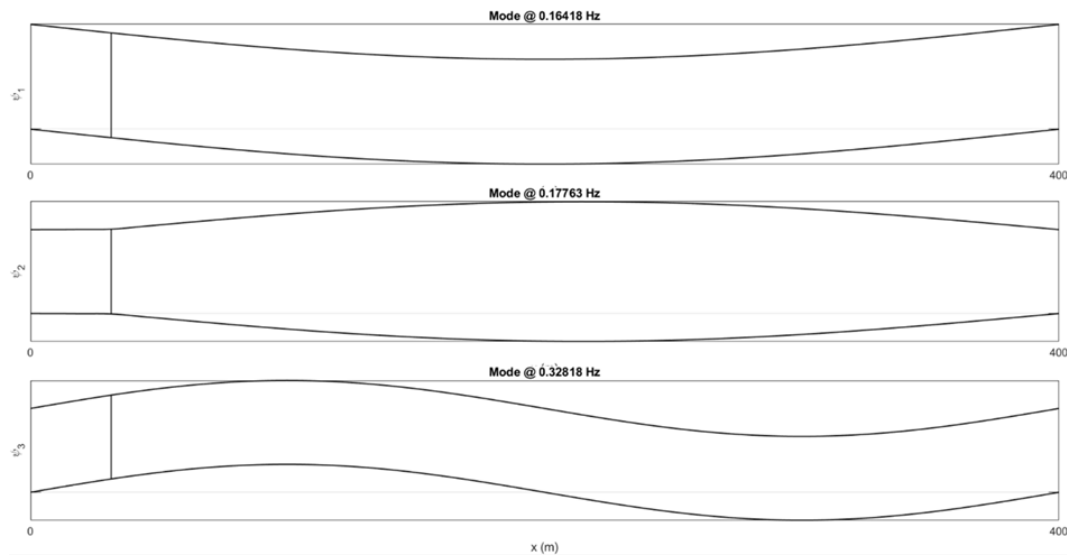


*Figure 18: one spacer-damper, first three modes*

Increasing the mode number, we can see that the frequencies increase as well, and the subspan behaviour becomes more complex. Figure 19 depicts the 23<sup>rd</sup>, 24<sup>th</sup> and 25<sup>th</sup> modes. Figure 19 shows the last three modes of the system (considering the modal truncation previously discussed).

As the frequency increase, higher modes develop more nodes, leading to more complex oscillation patterns. The presence of subspan oscillation is evident and could lead to localized stress concentrations. It's interesting that only even modes (2<sup>nd</sup>, 24<sup>th</sup> and 46<sup>th</sup>) have a subspan behaviour.

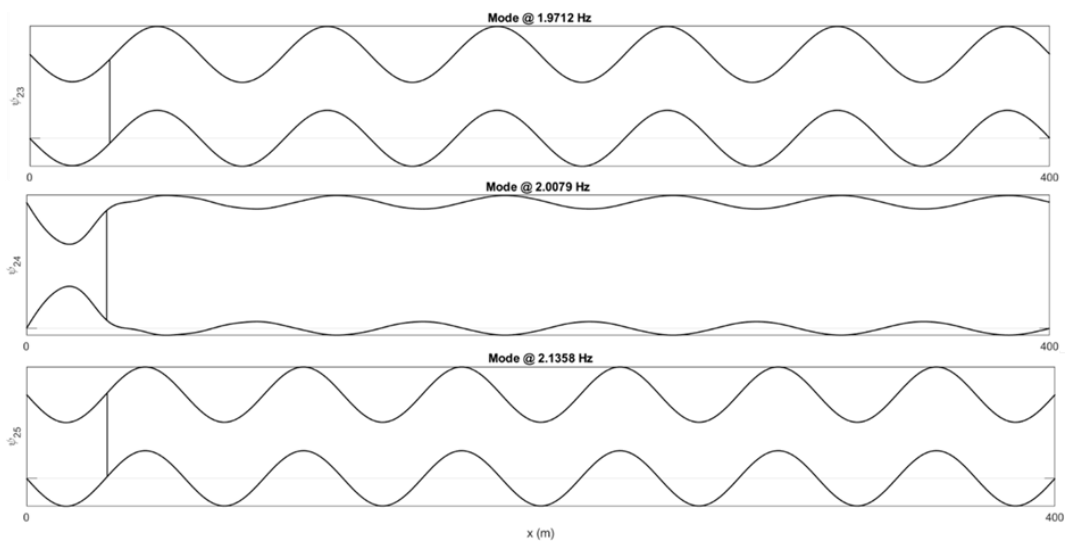


Figure 19: one spacer-damper, middle modes

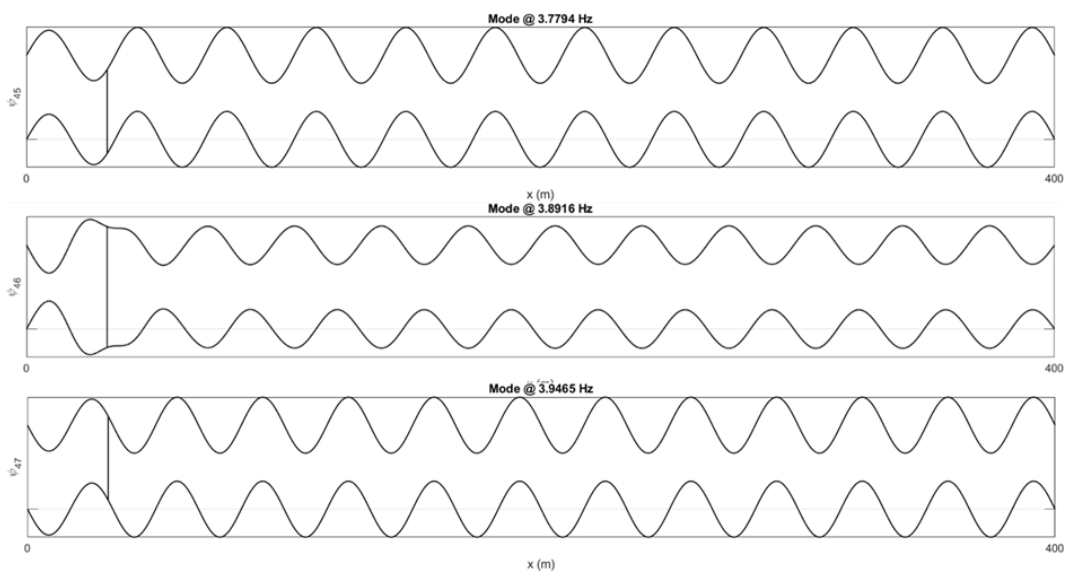
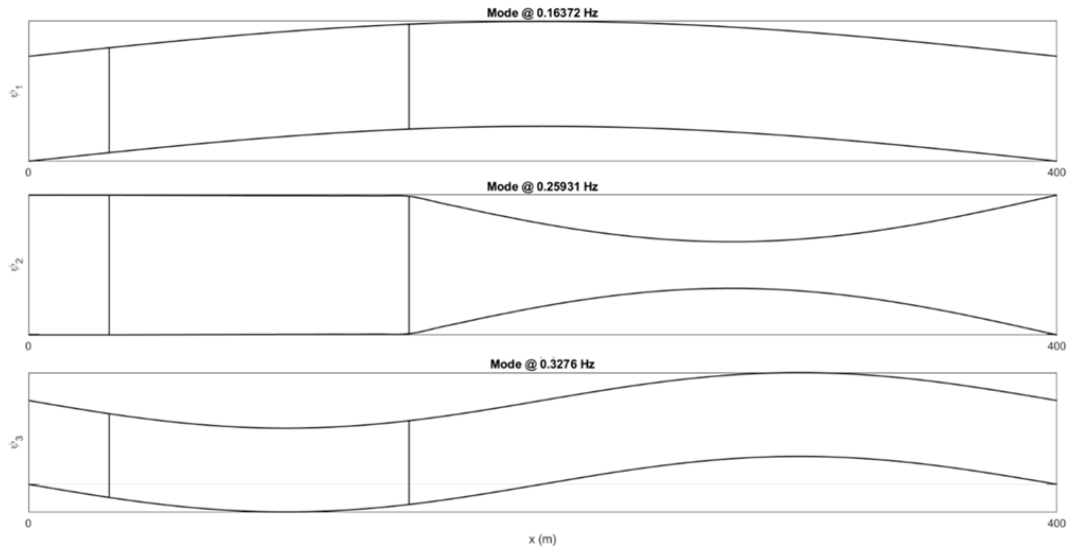


Figure 20: one spacer-damper, last three modes

- Two spacer-dampers

A second rigid spacer is here added at 148 m from the left end of the conductors. The first three modes of the systems are shown in Figure 21. The second mode has a subspan shape only in the right span. It already shows a better behaviour than single spacer case because the area between spacer remains still.



*Figure 21: two spacer-dampers, first three modes*

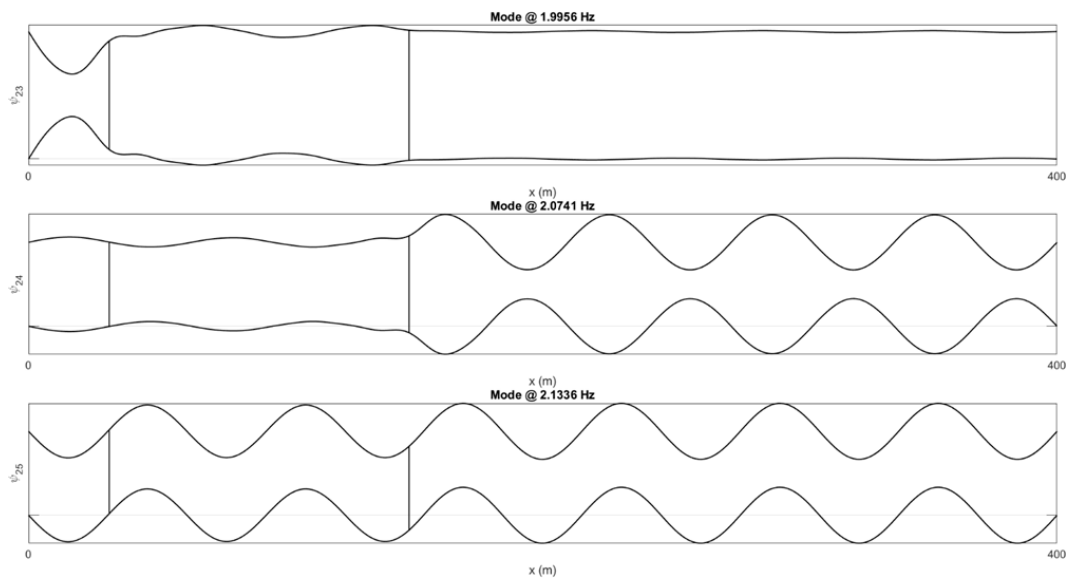


*Figure 22: two spacer-dampers, middle modes*

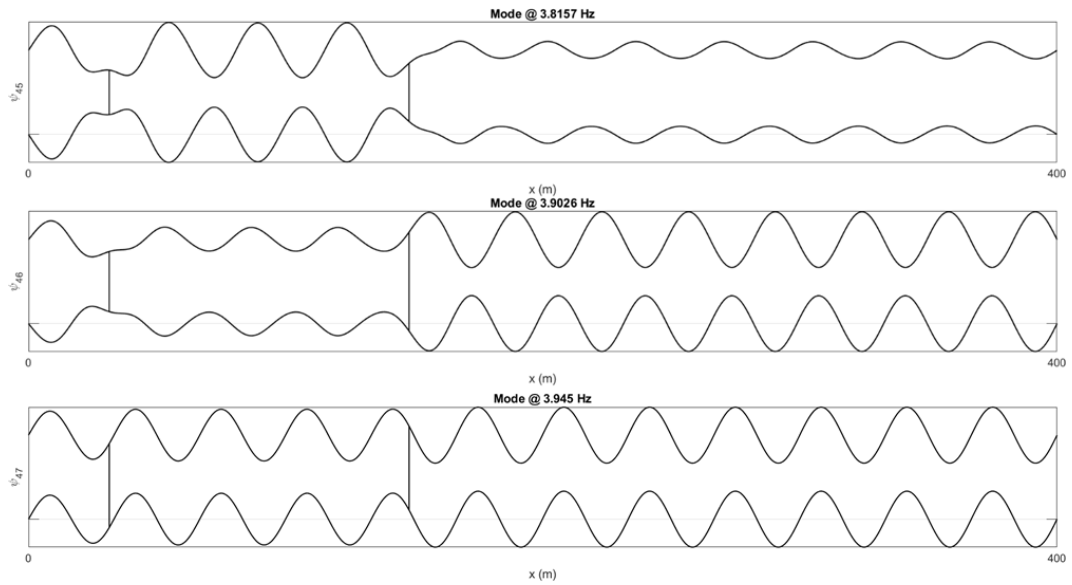


Figure 23: two spacer-dampers configuration, last three modes

- Real subspan positioning

In this case we put 7 spacers following the actual use made by Bertolotti. In the first three modes, showed in Figure 24, the cables move synchronously.

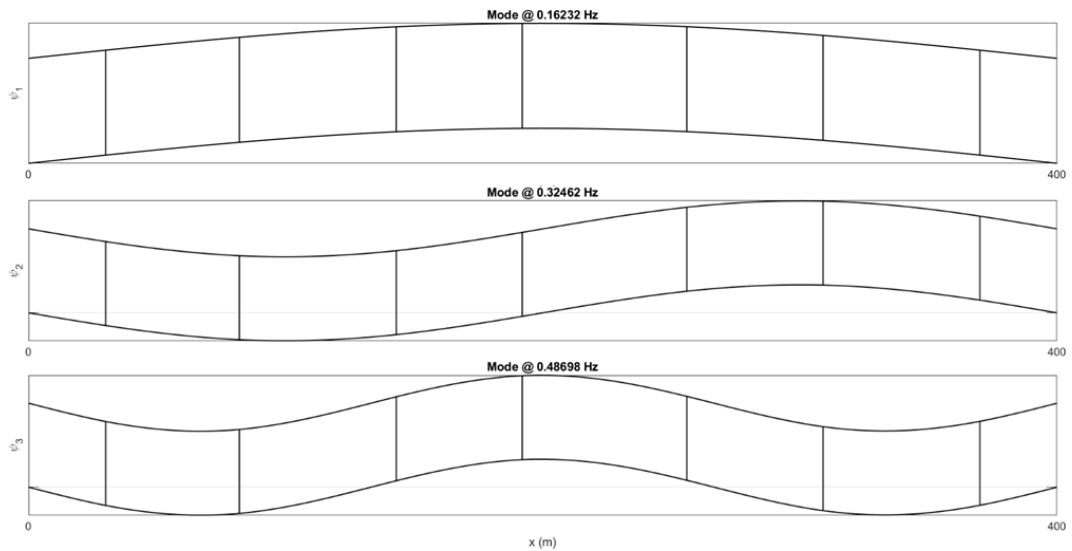
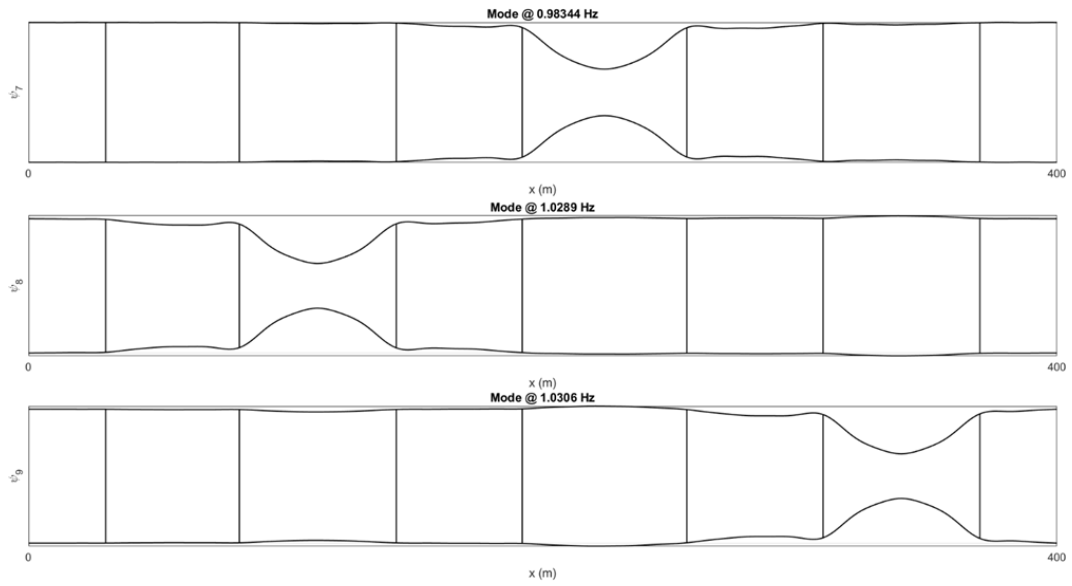
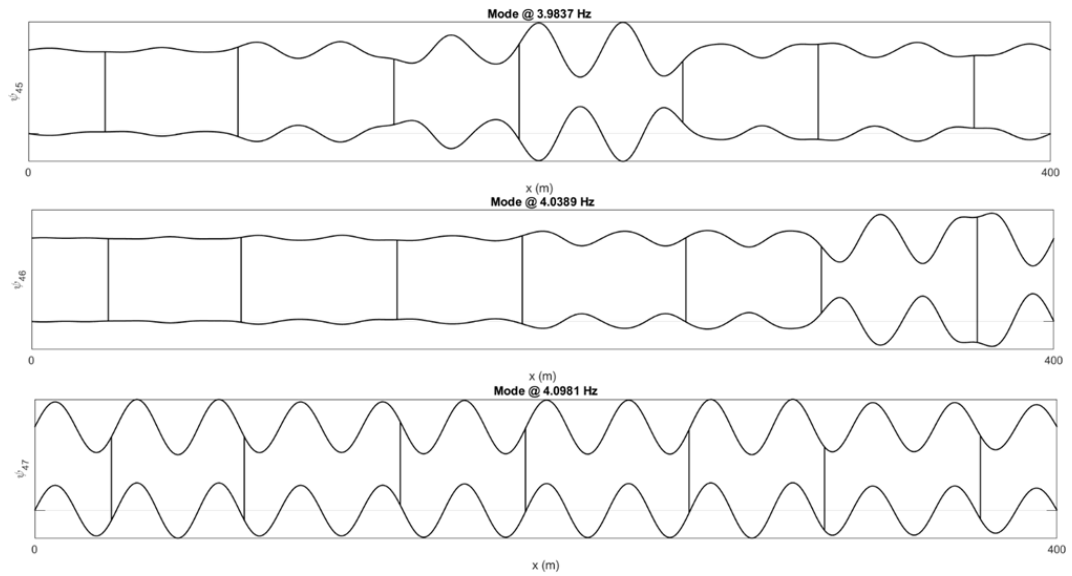


Figure 24: seven spacer-dampers, first three modes



*Figure 25: seven space-dampers, subspan modes*

The first subspan mode occurs at 7<sup>th</sup> mode at around 1 Hz. Then, we can see that in this range of frequency modal shapes are the same with the only difference that subspan phenomenon presents in a different span.



*Figure 26: seven space-dampers, last three modes*

Figure 26 shows that two of the last three modes presents subspan oscillations.

## 5.1.2 Variation of the spacer-damper stiffness $k_{AB}$

- Rigid connection

Let us consider again the single spacer case, with a rigid connection at 52 m. In this condition, there is no differences between  ${}_A w$  and  ${}_B w$  in correspondence of the spacer, as expected (Figure 27). Interestingly, on the left side of the spacer the cable B moves more than the cable A. While on the right side is the opposite.

In random point inside the span, Figure 28, we can see that the energy is gradually transmitted to the second cable (B).

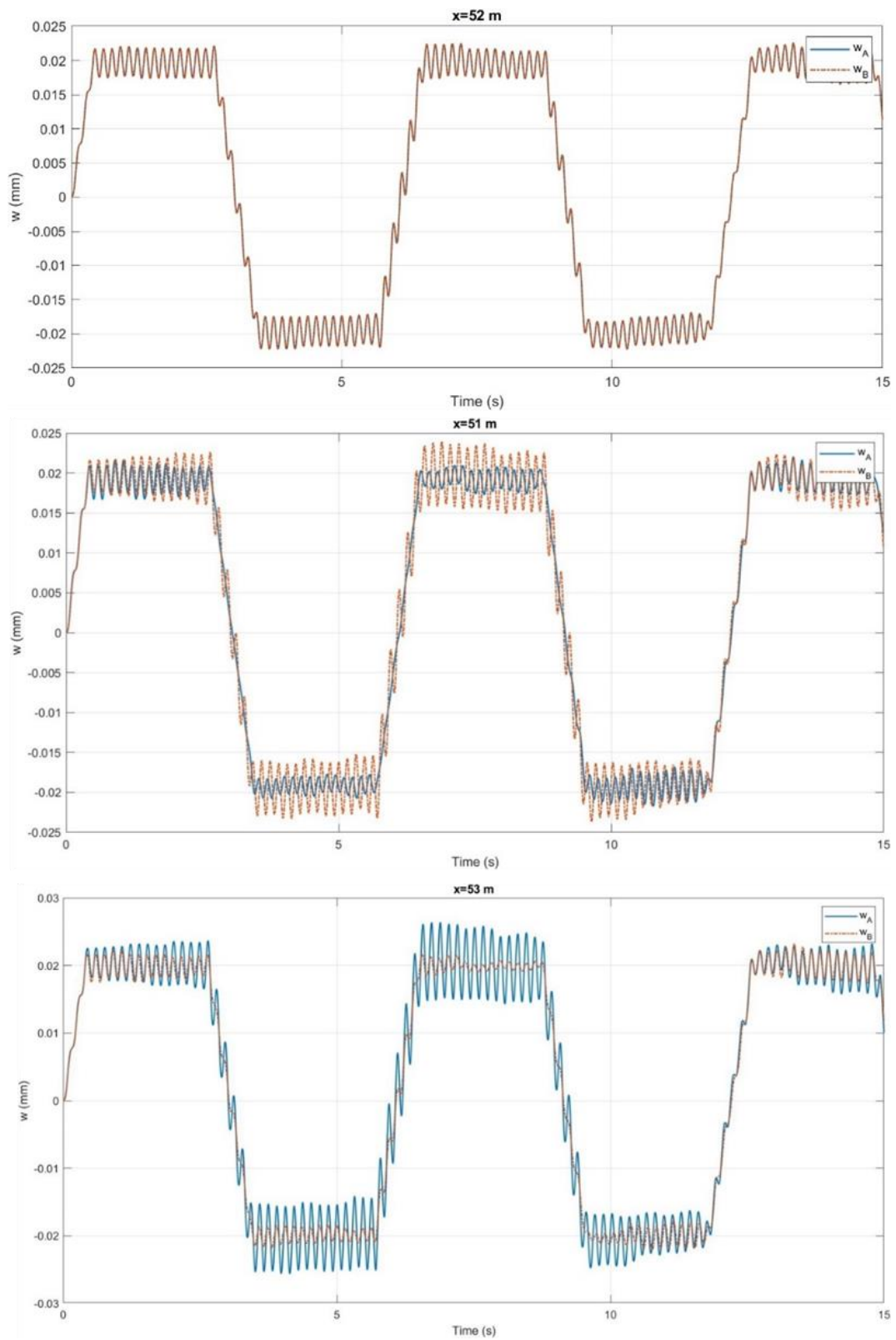


Figure 27: Rigid connection, node of joint and closer nodes

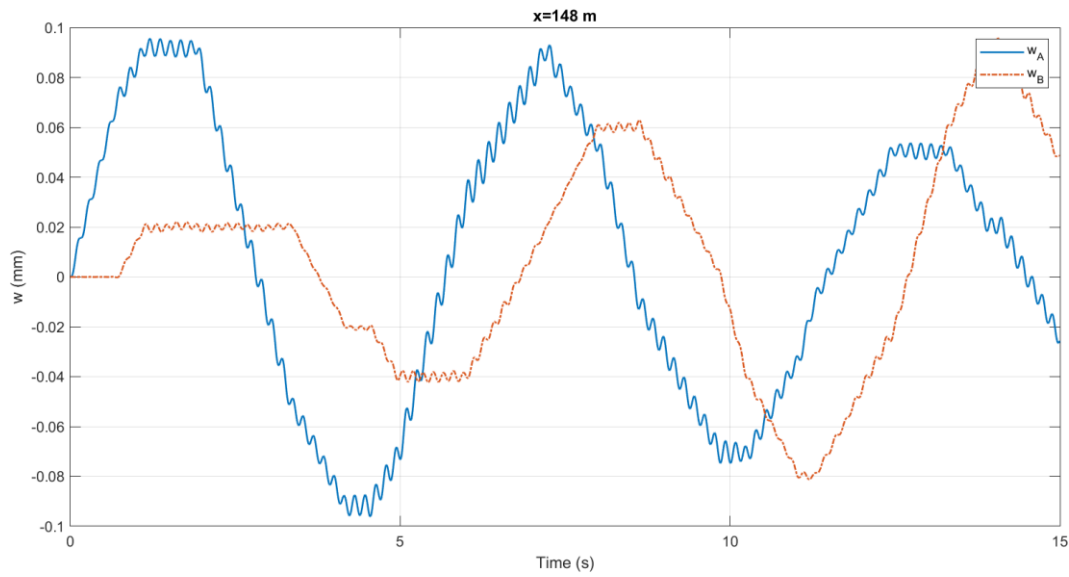


Figure 28: Rigid connection, random node

- Bertolotti spacer-damper

The spacer now is still located at 52 m, but the connection is flexible (see Chapter 3.2). In fact, according to Figure 29, the cable A presents a higher displacement w.r.t. B in correspondence of the spacer, and cable B receive the information with some delay.

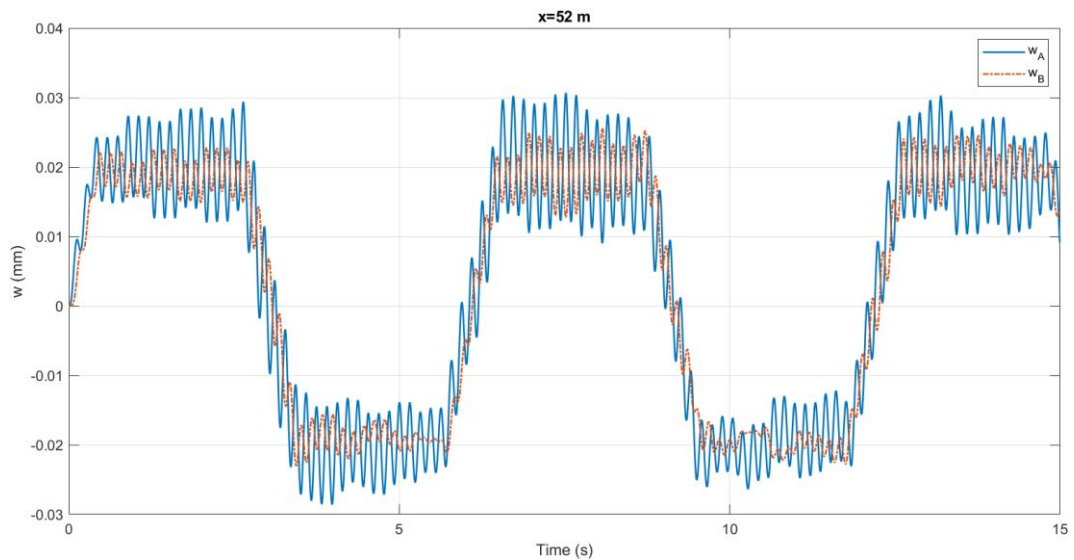


Figure 29: Spacer damper, node of joint

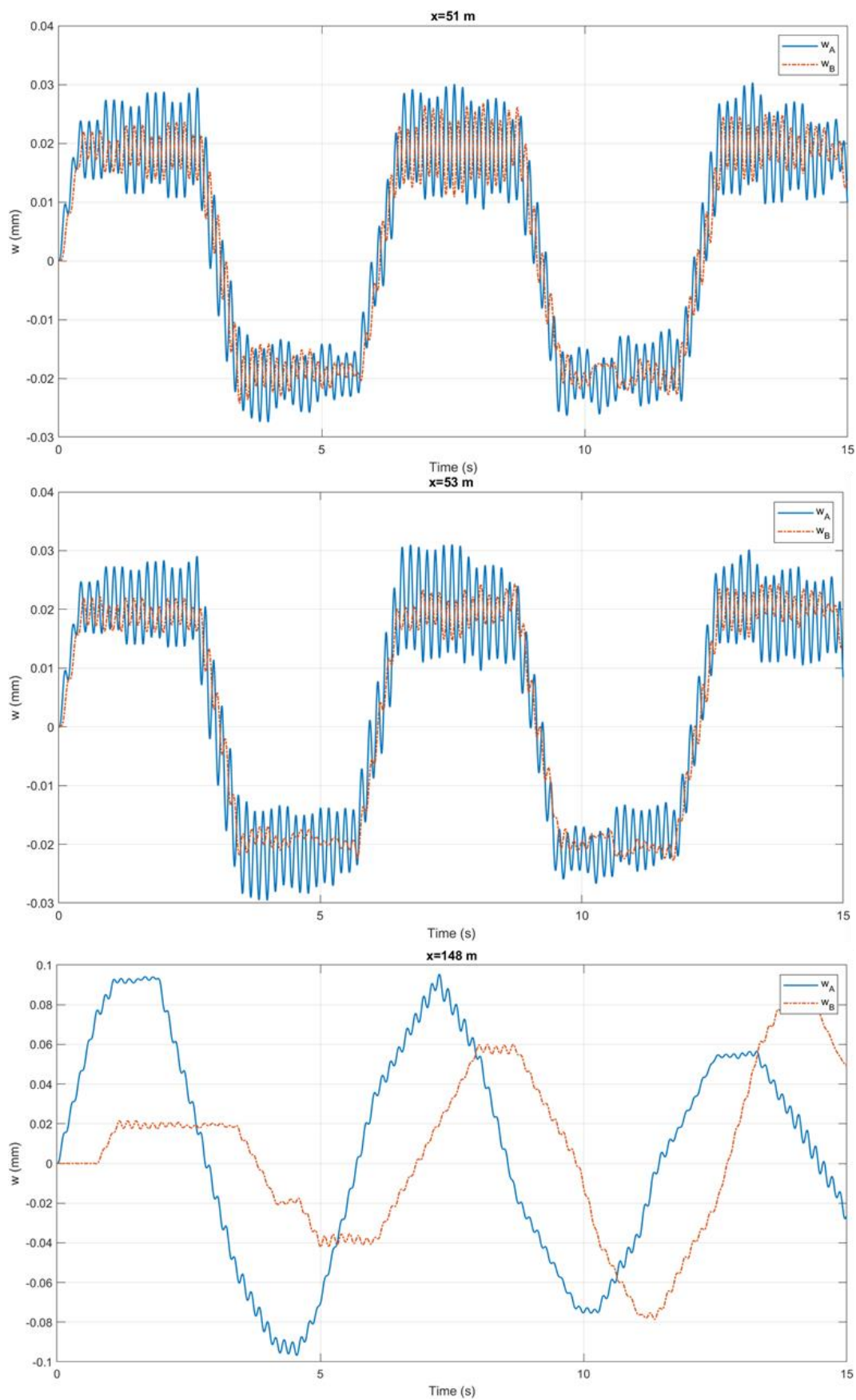


Figure 30: Spacer damper, nodes close to join and random node

### 5.1.3 Variation of the conductor pulling force $T$

In this case, we vary the axial stiffness between three values which are percentages of the load breaker  $RTS$ :

$$\begin{cases} S = 15\% RTS \\ S = 20\% RTS \\ S = 25\% RTS \end{cases}$$

The stiffness and position of the spacer are kept constant, as well as the force applied to the conductors. The results will be discussed considering the connection node and middle span node.

Figure 31 shows the effect of the axial tension in the connection node of the two conductors. Increasing the tension results in higher oscillations between higher and lower position. Since the tension influences the speed of the flexural waves on the conductors, the oscillatory pattern is also different with different values of  $S$ .

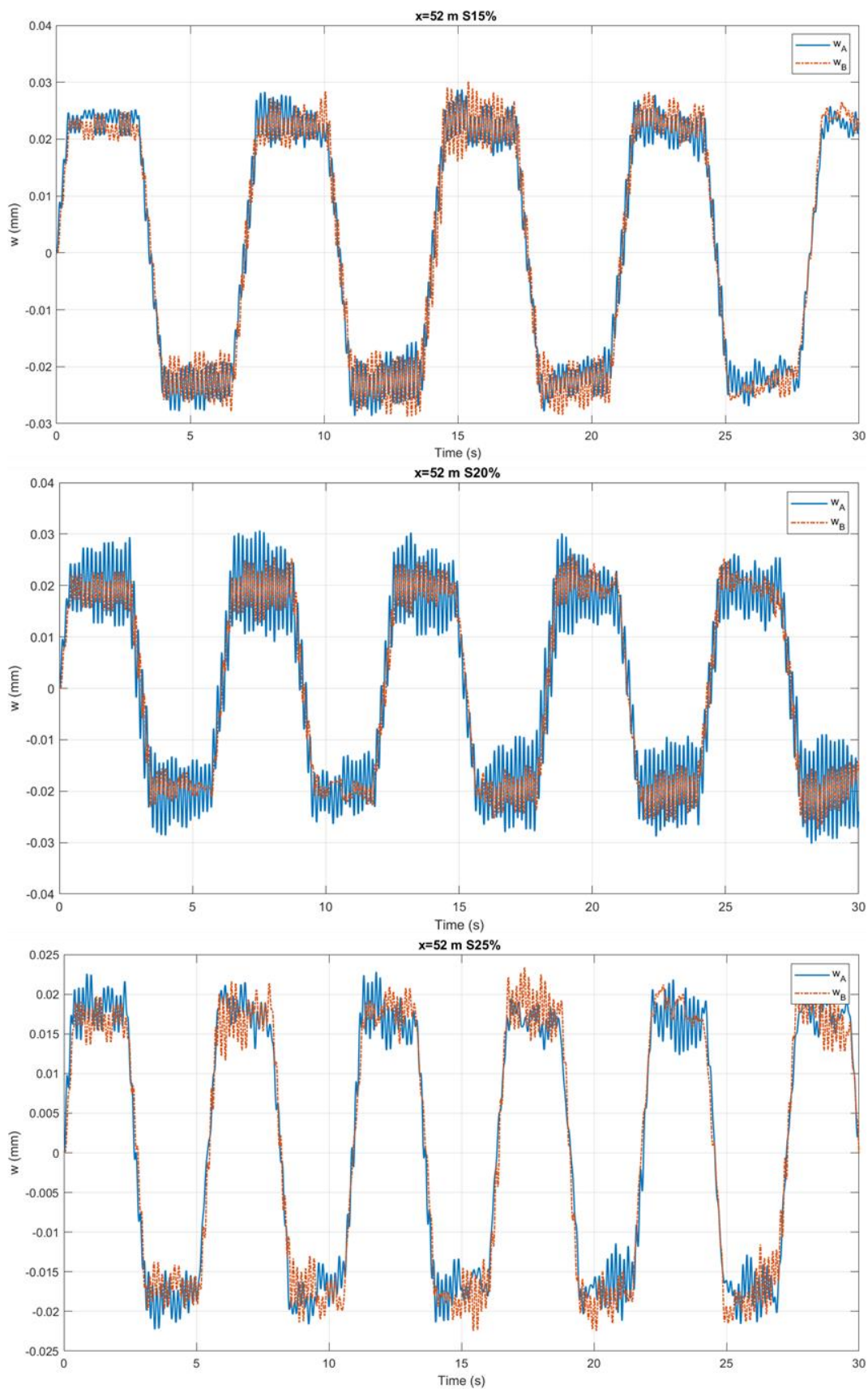


Figure 31 Node of connection: 15%,20%,25% Tensioned

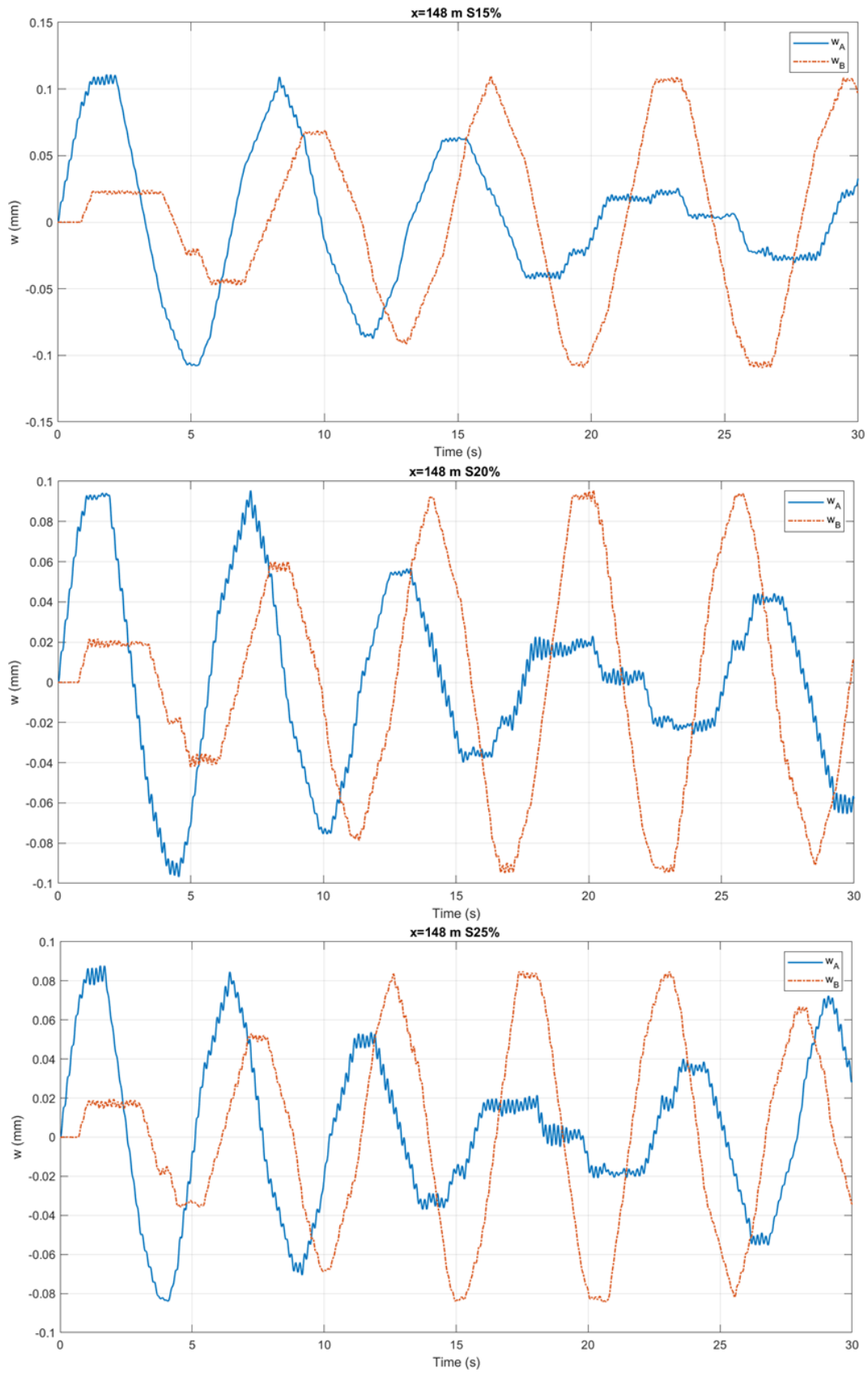


Figure 32: Midspan node: 15%,20%,25% Tensioned

### 5.1.4 Variation of the external force magnitude $F_c$

In this case, we vary the force module between three values:

$$\begin{cases} F = F_c \\ F = 10F_c \\ F = 100F_c \end{cases}$$

Maintaining constant stiffness and position of the spacer and axial tension. We analyse the results of the node of connection. As illustrated in Figure 33, the displacement of the first graph is multiplied by 10 and 100 in the second and third graph respectively. Since the model considered in this thesis is linear, the displacements  $w_A$  and  $w_B$  are directly proportional to the magnitude  $F_c$ .

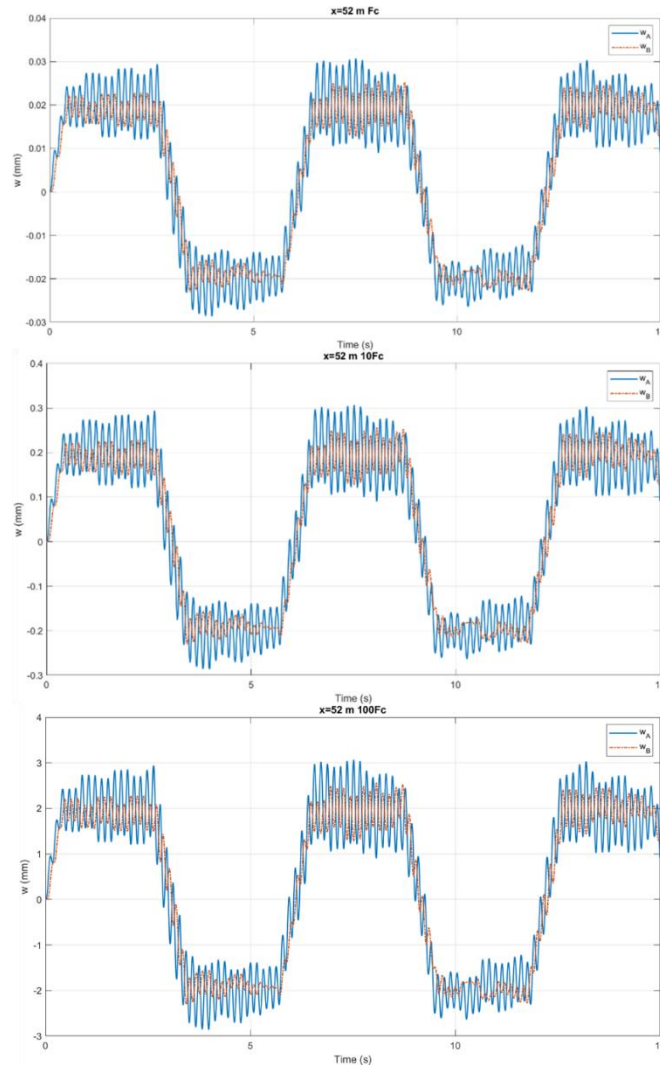


Figure 33: Variation of force module

### 5.1.5 Variation of wind velocity $v$

Wind velocity is an important factor also to be analysed. Increasing velocity, increase also the frequency of excitation. So, we'll have more modes to describe the time response. We are interested in these ranges of velocity:

$$\left\{ \begin{array}{l} \textit{Aeolian} \quad v = 1 : 8 \frac{m}{s} \\ \textit{Subspan} \quad v = 8 : 20 \frac{m}{s} \end{array} \right.$$

Taking in consideration the maximum and the minimum value of each of these ranges, we'll take them as study parameters:

$$\left\{ \begin{array}{l} v = 1 \frac{m}{s} \\ v = 8 \frac{m}{s} \\ v = 20 \frac{m}{s} \end{array} \right.$$

As shown in Figure 34 and Figure 35, the maximum and minimum values of  $w$  increase with velocity, indicating that stronger wind excitation leads to larger oscillations. As expected, the number of oscillations per unit time grows as velocity increases.

At higher velocities, the response pattern becomes more distinct, with sharper transitions between peaks and troughs. This suggests that more vibration modes are contributing to the overall motion.

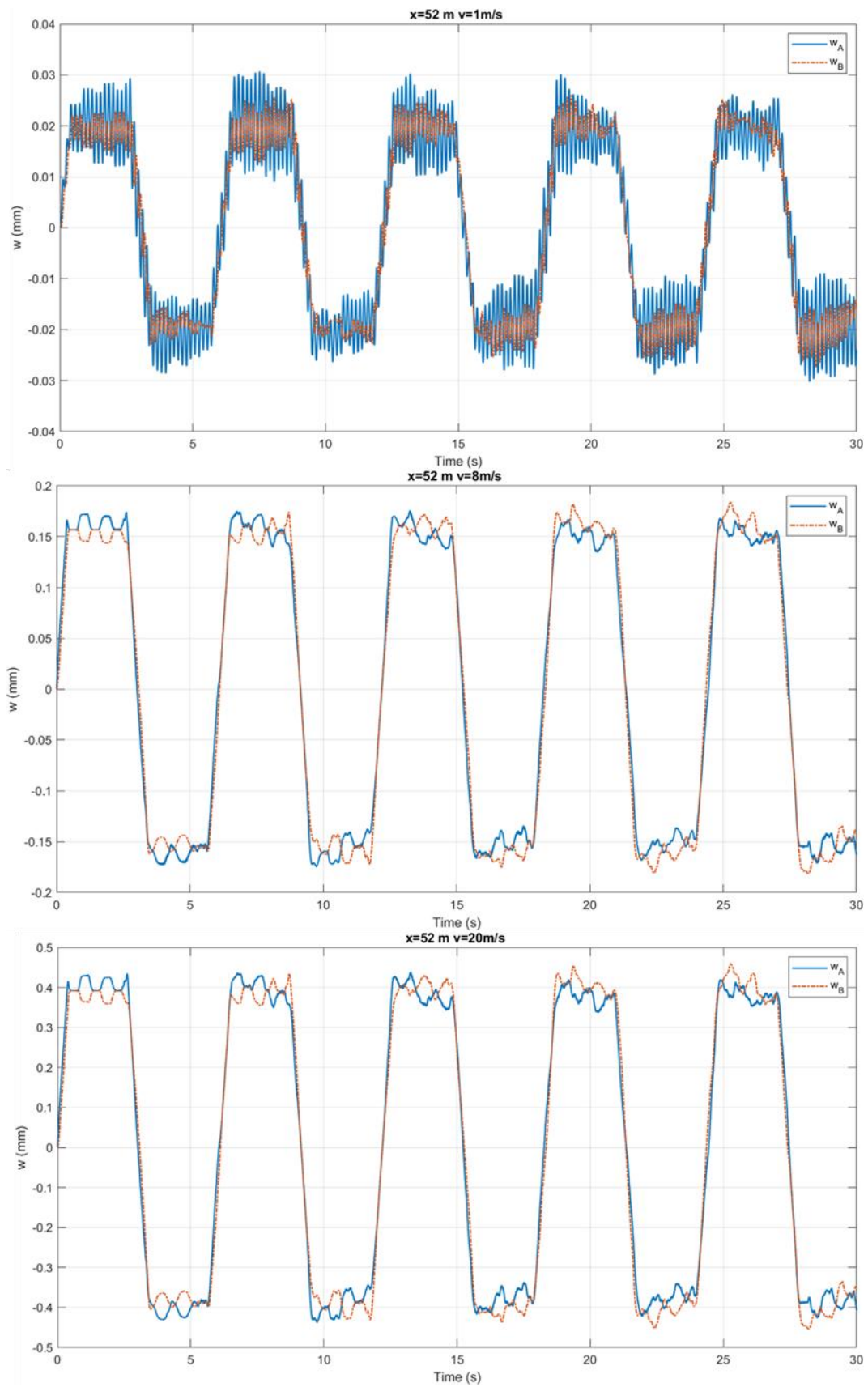


Figure 34: Variation of wind velocity, node of connection

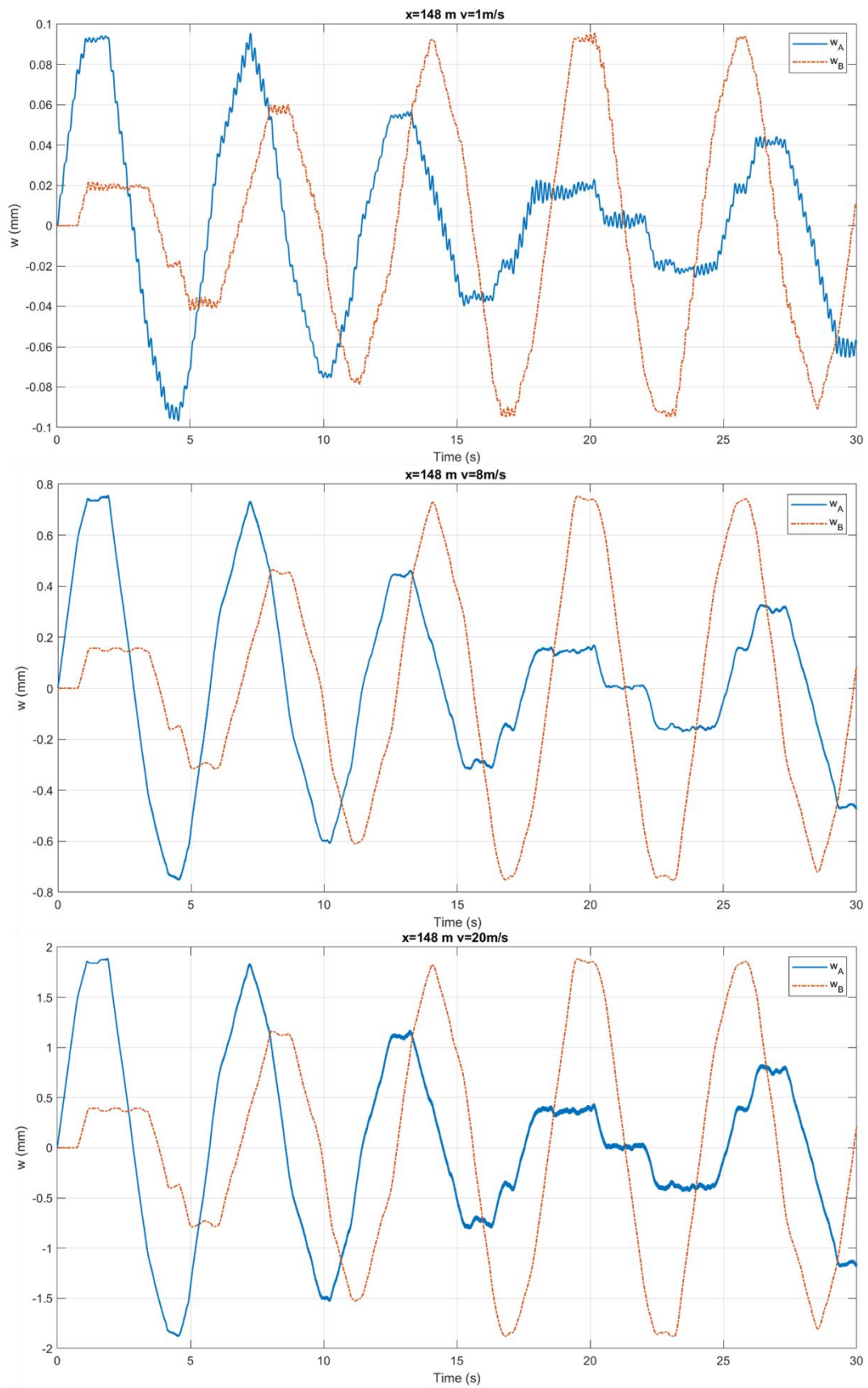


Figure 35: Variation of wind velocity, midspan node

### 5.1.6 Variation of spacer damper mass $m_{AB}$

The mass of the Bertolotti spacer damper is:

$$m_{AB} = 5.2 \text{ kg}$$

To understand the influence of the mass on the system displacement, we add two other orders of magnitude:

$$\begin{cases} m_{AB} = 0.52 \text{ kg} \\ m_{AB} = 5.2 \text{ kg} \\ m_{AB} = 52 \text{ kg} \end{cases}$$

From the plots, Figure 36 and Figure 37, it is evident that as the mass of the spacer damper increase, the displacements appear smoother, with reduced oscillatory behaviour. This suggests that the higher mass is effectively absorbing and dissipating vibrational energy. A heavier damper resists acceleration more, leading to a more stable response.

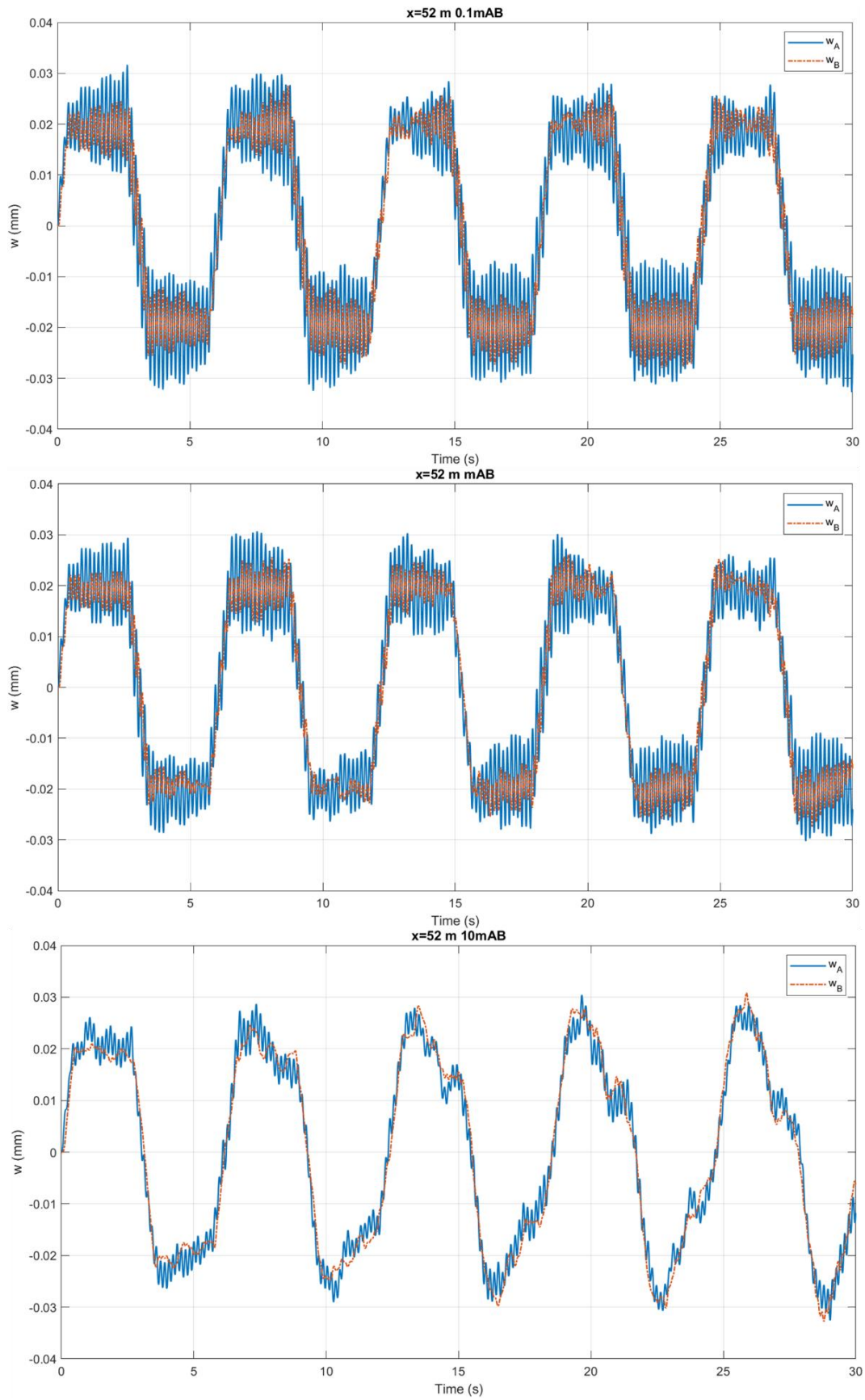


Figure 36 Variation of spacer's mass, node of connection

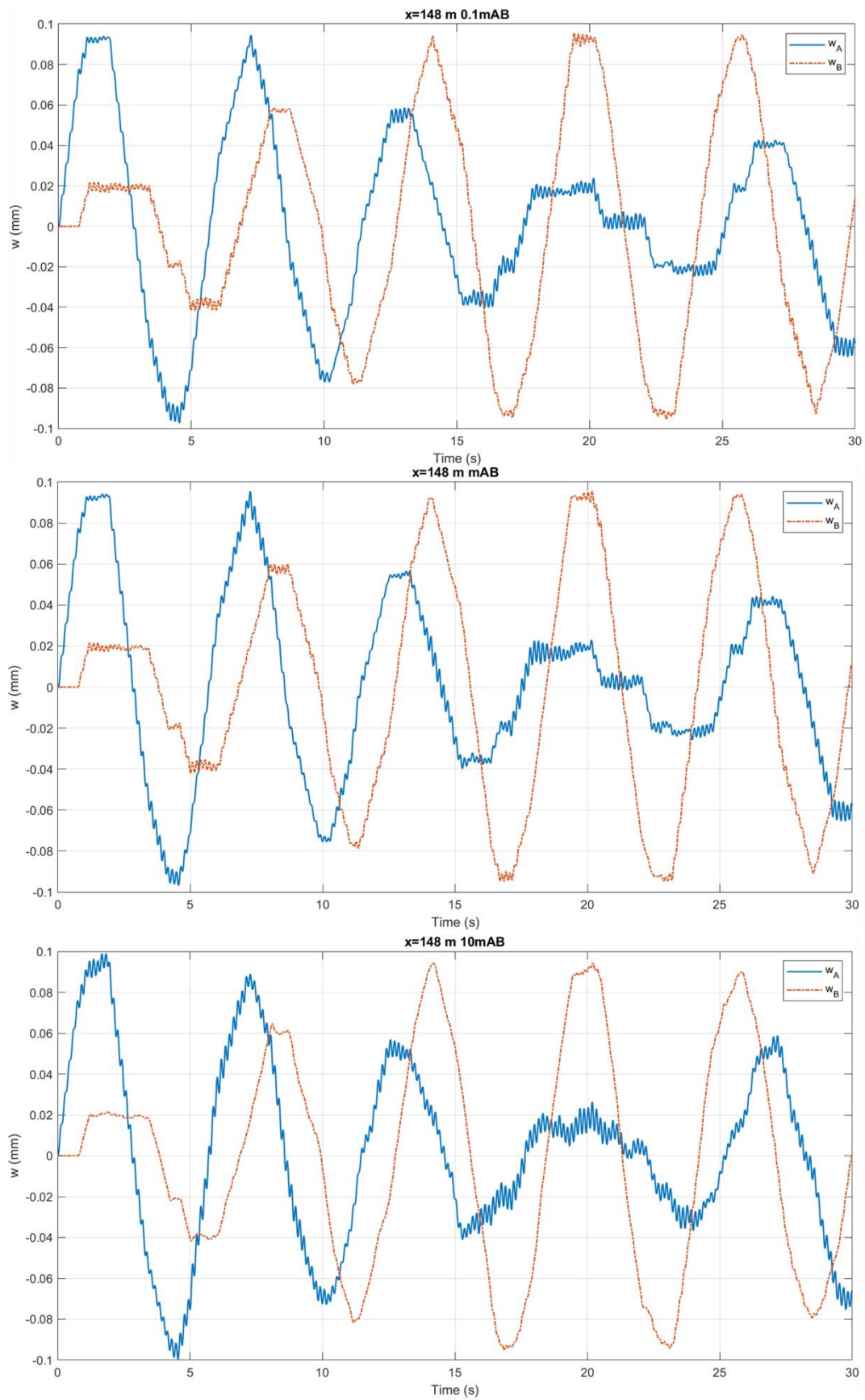
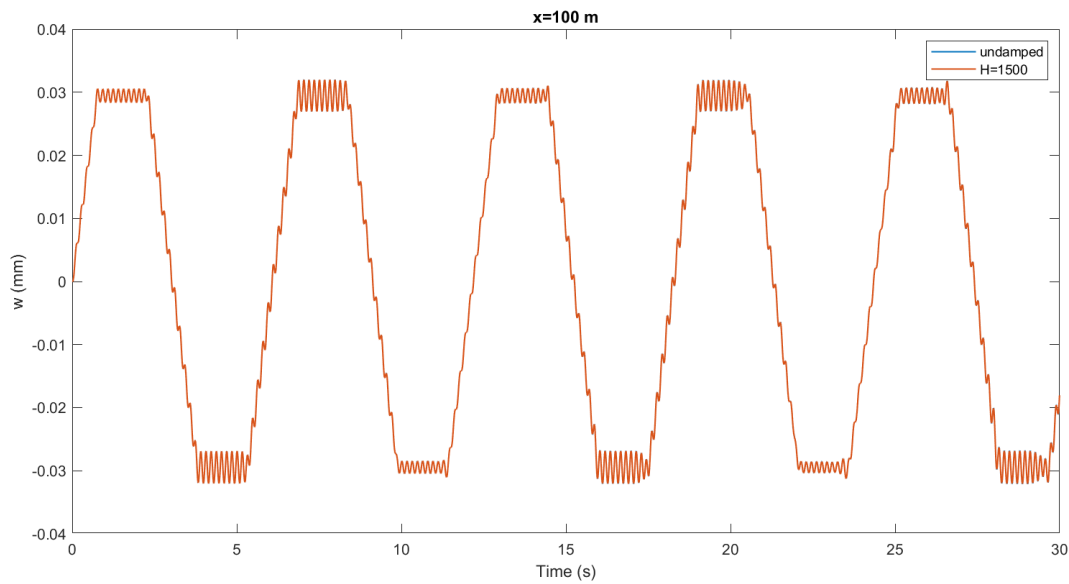


Figure 37: Variation of spacer's mass, midspan node

## 5.2 Damped conductors

Starting from the single conductor, we can add examples of time response with different value of the self-damping cable constant  $H$ . For  $H = 1500$ , damped and undamped solutions match: there is no evident dissipation of energy (Figure 38).



*Figure 38: Displacement, undamped and with  $H=1500$*

We try other  $H$  of higher orders.

$$\begin{cases} H = 15000 \\ H = 150000 \end{cases}$$

In these cases, as we can see in Figure 39, dissipation phenomena start to appear. To observe the effectiveness of this model we try to simulate double conductors with self-damping. Variation of self-damping coefficient  $H$  is taken into study.

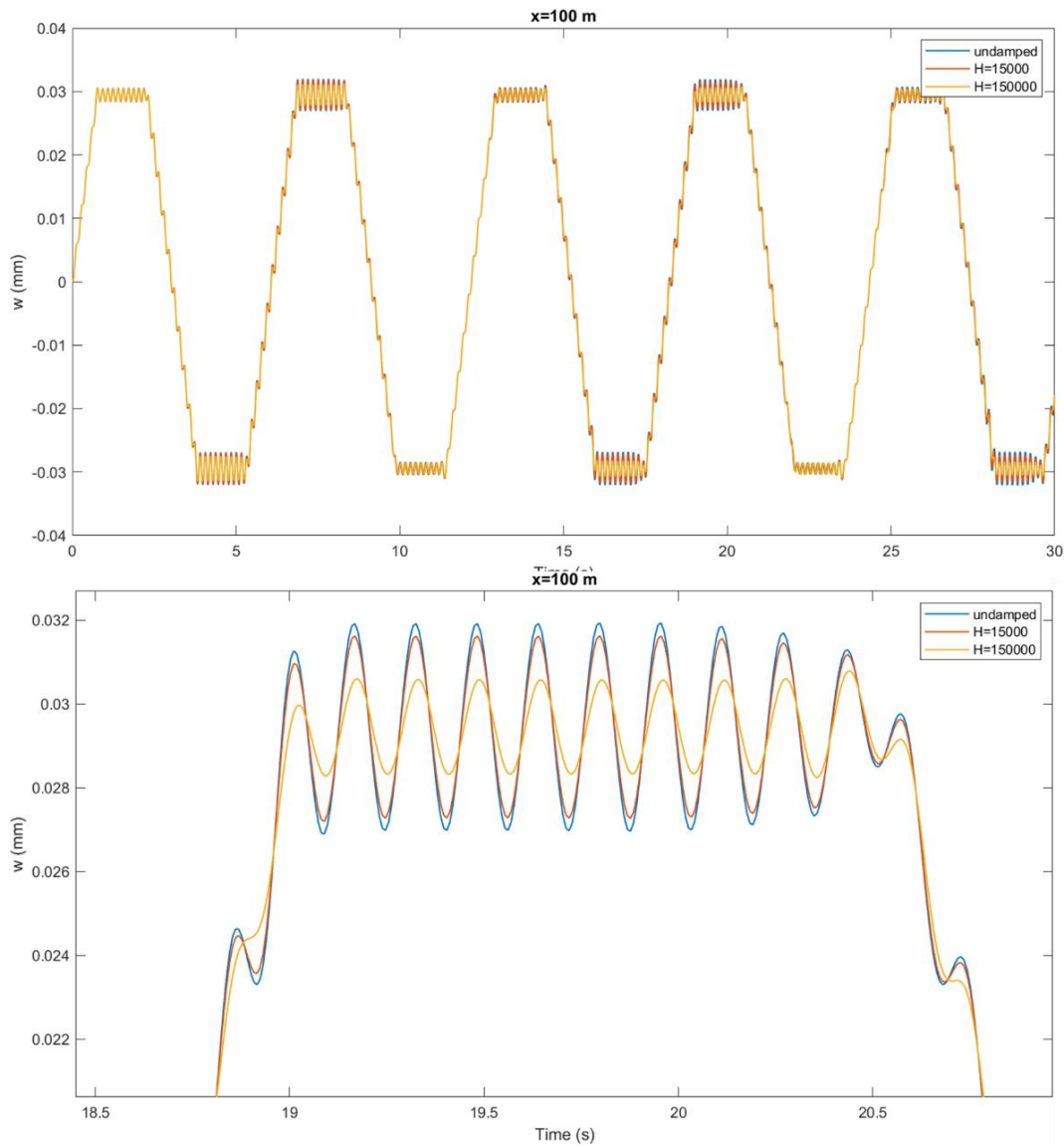


*Figure 39: Displacement with different values of  $H$*

### 5.2.1 Effect of the self-damping coefficient on coupled cables

Considering the same coupled configuration introduced in Section 5.1, we plot these cases of  $H$ :

$$\left\{ \begin{array}{l} \text{undamped} \\ H = 1500 \\ H = 15000 \\ H = 150000 \end{array} \right.$$

In the node of connection, we have the graphs below. As we expected there is no evident difference between *undamped* and  $H = 1500$ . Increasing  $H$ , the oscillation of both cables decreases after 10 seconds.

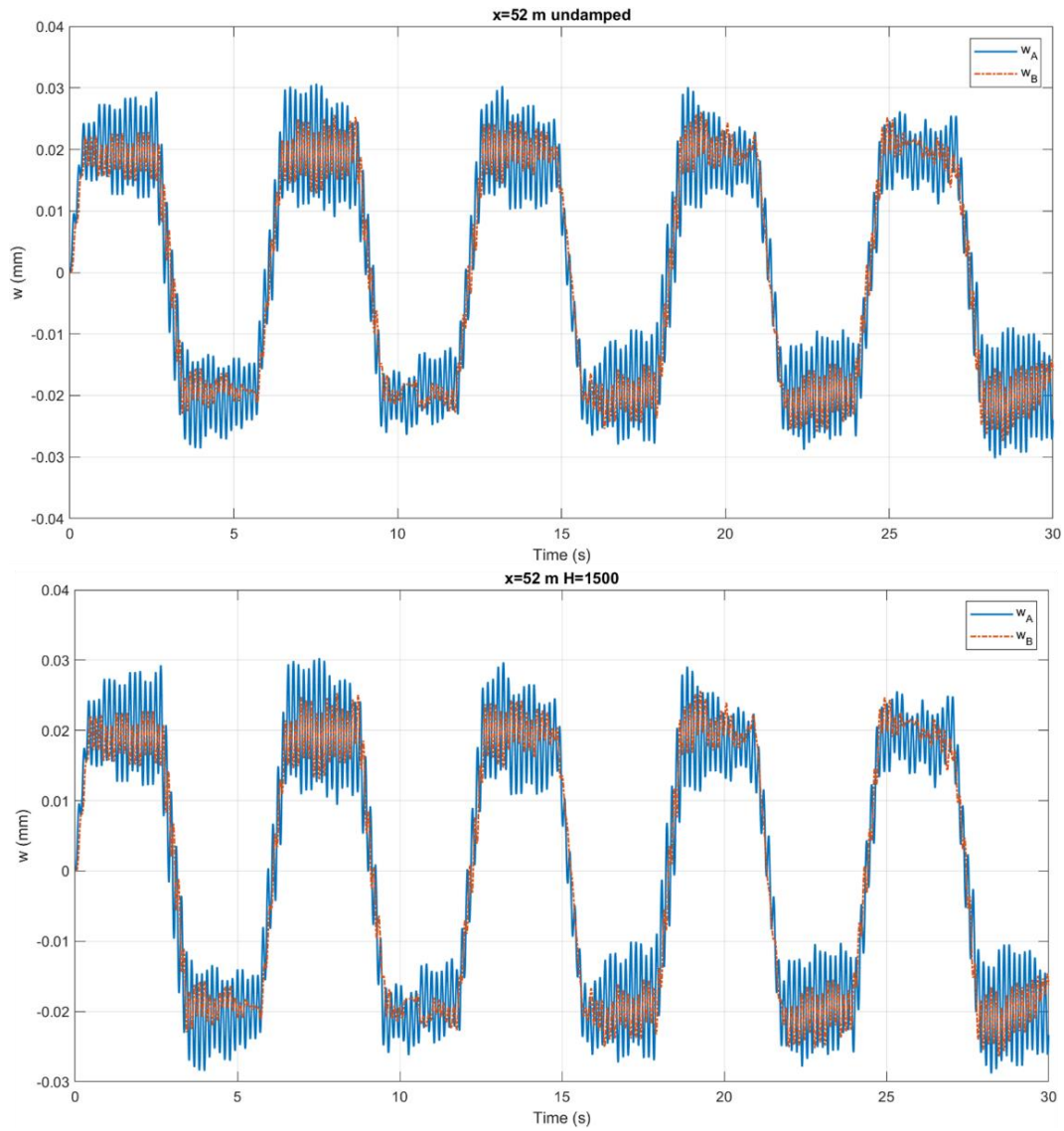


Figure 40: Couple conductor displacement, undamped and  $H=1500$

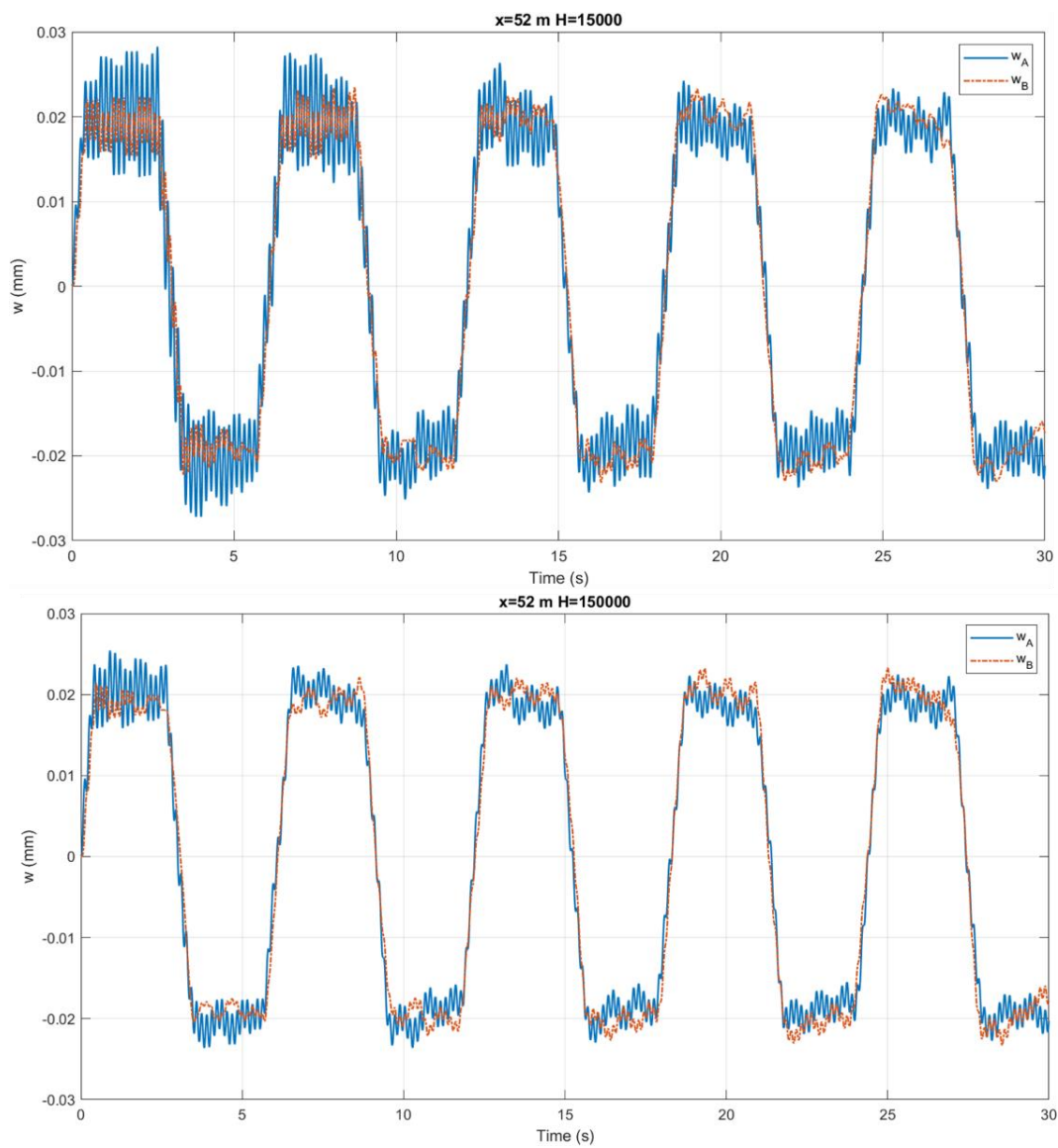


Figure 41: Couple conductor displacement,  $H=15000$  and  $H=150000$

## 6 Conclusion

The present thesis aimed at studying the dynamical behaviour of single and coupled conductors, considering a single span of an overhead line.

After a general overview of the background given in Chapter 1, the modal analysis of the conductor basic model (i.e. the Euler-Bernoulli beam) started in Chapter 2. Here the set-up of the theoretical problem was done: the solution obtained for pinned-pinned constraints was used for the further improvements on the basic model.

The problem was made more realistic adopting a taut Euler-Bernoulli beam with self-damping and external excitation. With the same boundary conditions, it was shown the effect of the tensioning on the modal parameters. This equation was at the base for the coupled configuration.

In Chapter 3, a model of two coupled conductors was introduced. The beams were linked by elastic spacers with lumped masses and stiffness equivalent to a real spacer-damper proper for the analysed conductors. The general solution was obtained using the Ritz-Galerkin method, and both the modal parameters and a time solution of the beams were derived.

In Chapter 4, the Matlab coded to plot the results was presented. The script was run with different number of modes  $N$ , in order to adequately define it for describing the solution: the convergence of the solution was verified both in the single conductor case and for the coupled conductors.

In Chapter 5, the modal shapes of the coupled conductors were shown and discussed. The time response of the system was checked at different points on the span through a sensitivity analysis of the main parameters: number of spacer-dampers, their stiffness, external force amplitude, cable tensioning and self-damping are investigated for different magnitudes to see the effect on system output given the same input and verifying the very low sensitivity to cable self-damping.

Further analysis could be focused on the spacer-dampers damping effect, but they need a different representation due to the out diagonal terms in the damping matrix. Another interesting development would be the study of conductors bundle as triple, quad, hexa etc. those are of current use in the overhead lines, together with the real wind excitation coming from lab tests. The distribution of the wind (i.e. the force) can be used to determine the real strain field on the conductors of the bundle, making possible a prediction of the fatigue behaviour and a life estimation of the line.

## APPENDIX

### Appendix A – Euler-Bernoulli beam

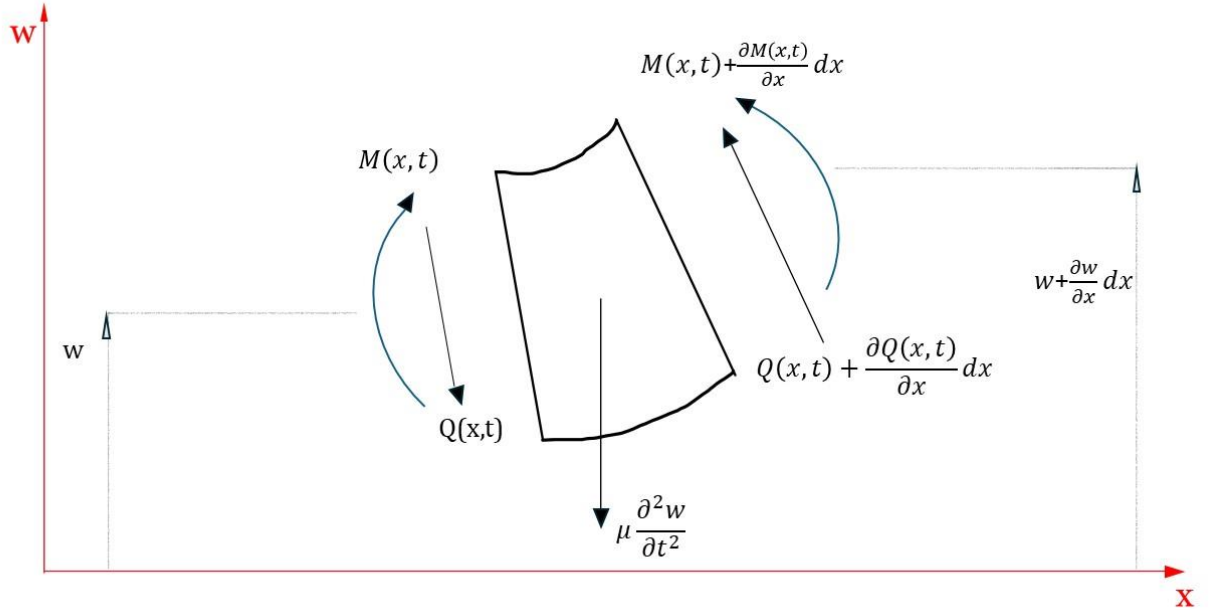


*Figure 42: free-body diagram for a beam element*

Figure 42 shows the free-body diagram for a beam element of length  $dx$  of the conductor. The quantity  $w(x, t)$  denotes the transverse deflection.  $Q, M$  are the shear force and bending moment acting at the left-end side of the conductor element.  $Q + dQ, M + dM$  are applied on the right-end side. The term  $\mu \frac{\partial^2 w}{\partial t^2}$  is the inertial force due to the motion of the element itself. This is the only inertial force we consider since the rotatory inertia of the cross-section can be neglected under the hypothesis of Euler-Bernoulli beam theory of no shear deformation. This is the transversal equilibrium:

$$\left( Q + \frac{\partial Q}{\partial x} dx \right) - Q = \mu \frac{\partial^2 w}{\partial t^2} dx$$

$$\frac{\partial Q}{\partial x} dx = \mu \frac{\partial^2 w}{\partial t^2} dx$$

The shear force  $Q(x)$  is related to the bending moment  $M(x, t)$  by:  $Q(x) = \frac{\partial M}{\partial x}$ .

Being:  $M(x) = -EI \frac{\partial^2 w}{\partial x^2}$

We can write that  $Q(x) = -EI \frac{\partial^3 w}{\partial x^3}$

Substituting in the general equation we obtain:

$$-EI \frac{\partial^4 w}{\partial x^4} dx = \mu \frac{\partial^2 w}{\partial t^2} dx$$

Dividing by  $dx$  and rearranging:

$$\mu \frac{\partial^2 w}{\partial t^2} + EI \frac{\partial^4 w}{\partial x^4} = 0$$

## Appendix B – Eigenfunctions calculation

We explore the circumstances under which the motion of the beam is synchronous, meaning that every point of the beam executes the same motion in time, passing through equilibrium at the same time and reaching the maximum excursion at the same time. Follows that during synchronous motion the beam exhibits a certain unique profile, or general shape, and the profile doesn't change with time, only the amplitude of the profile does. Such a solution  $w(x, t)$  is said to be separable in the spatial variable  $x$  and time  $t$ , and can be expressed in the form:

$$w(x, t) = \Phi(x)\eta(t)$$

Where  $\Phi$  represents the shape and  $\eta$  represents how the amplitude of the shape varies with time.

Rewriting the partial equation:

$$-\eta(t) \frac{\partial^2}{\partial x^2} \left( EI(x) \frac{\partial^2 \Phi(x)}{\partial x^2} \right) = \mu(x) \Phi(x) \frac{\partial^2 \eta(t)}{\partial t^2}$$

Dividing by  $\eta(t)\mu(x)\Phi(x)$ :

$$-\frac{1}{\mu(x)\Phi(x)} \frac{\partial^2}{\partial x^2} \left( EI(x) \frac{\partial^2 \Phi(x)}{\partial x^2} \right) = \frac{1}{\eta(t)} \frac{\partial^2 \eta(t)}{\partial t^2} = \lambda$$

Observing that the left side depends only on  $x$  and the right side only on  $\eta$ , we conclude that the solution  $y(x, t)$  is indeed separable [6]. Both sides must be equal to a constant  $\lambda$ . To see the nature of that constant we consider only the right side:

$$\frac{\partial^2 \eta(t)}{\partial t^2} - \lambda \eta(t) = 0$$

Which solution has an exponential form:

$$\eta(t) = Ae^{st}$$

So, substituting in the previous equation and dividing through by  $Ae^{st}$ :

$$s^2 - \lambda = 0$$

With solutions, assuming  $\lambda = -\omega^2 < 0$ , are:

$$\begin{cases} s_1 = \sqrt{\lambda} = i\omega \\ s_2 = -\sqrt{\lambda} = -i\omega \end{cases}$$

$$\eta(t) = A_1 e^{i\omega t} + A_2 e^{-i\omega t}$$

$\eta(t)$  represents an harmonic oscillation, so we can write:

$$\eta(t) = C \cos(\omega t - \phi)$$

Where  $C$  is an amplitude,  $\phi$  a phase angle and  $\omega$  the frequency of oscillation.

Now, we can find the displacement configuration  $\Phi(x)$  assumed by the beam.

$$\frac{\partial^2}{\partial x^2} \left[ EI(x) \frac{\partial^2 \Phi(x)}{\partial x^2} \right] = \omega^2 \mu(x) \Phi(x)$$

Considering  $I(x)$  constant along the beam:

$$\frac{\partial^4 \Phi(x)}{\partial x^4} - \beta^4 \Phi(x) = 0 \quad \text{where } \beta^4 = \frac{\omega^2 m}{EI}$$

$$\Phi(x) = A \sin(\beta x) + B \cos(\beta x) + C \sinh(\beta x) + D \cosh(\beta x)$$

$$\frac{\partial^2 \Phi(x)}{\partial x^2} = \beta^2 [-A \sin(\beta x) - B \cos(\beta x) + C \sinh(\beta x) + D \cosh(\beta x)]$$

$$\left. \frac{\partial w^2(x, t)}{\partial x^2} \right|_{x=0}$$

Applying the boundary condition (pinned ends) we obtain:

$$\begin{cases} \Phi(0) = 0 & \rightarrow B + D = 0 \\ \left. \frac{\partial \Phi^2(x, t)}{\partial x^2} \right|_{x=0} = 0 & \rightarrow -B + D = 0 \end{cases} \rightarrow B = D = 0$$

$$\begin{cases} \Phi(L) = 0 & \rightarrow A \sin(\beta L) + C \sinh(\beta L) = 0 \\ \left. \frac{\partial \Phi^2(x, t)}{\partial x^2} \right|_{x=L} = 0 & \rightarrow -A \sin(\beta L) + C \sinh(\beta L) = 0 \end{cases}$$

$$\text{sum} \rightarrow 2C \sinh(\beta L) = 0 \rightarrow C = 0$$

At the end we get the characteristic equation:

$$\sin(\beta L) = 0$$

The solution is given by an infinite set of eigenvalues:

$$\beta_r L = r\pi \quad r = 1, 2, \dots$$

Substituting in the eigenfunction:

$$\Phi_r(x) = A_r \sin \beta_r x = A_r \sin \left( \frac{r\pi x}{L} \right)$$

Which results in an infinite set of eigenfunctions. These represent the vibrational characteristics of the beam under free vibration conditions. Each  $n$  corresponds to a different mode of vibration.

## Appendix C – Modal equation of Euler-Bernoulli beam

$$\mu \frac{\partial^2 w}{\partial t^2} + EI \frac{\partial^4 w}{\partial x^4} = 0$$

Assuming that the solution can be written as a series of mode shapes and time functions:

$$w(x, t) = \sum_{n=1}^{\infty} \Phi_n(x) \eta_n(t)$$

Substituting into the equation:

$$\mu \sum_{n=1}^{\infty} \Phi_n(x) \ddot{\eta}_n(t) + EI \sum_{n=1}^{\infty} \Phi_n^{IV}(x) \eta_n(t) = 0$$

Using the orthogonality of the mode shapes and multiplying by  $\Phi_m(x)$ . Integrating over  $x$  from 0 to  $L$ , we obtain the equation:

$$\int_0^L \mu \ddot{\eta}_n(t) \Phi_n(x) \Phi_m(x) dx + \int_0^L EI \eta_n(t) \Phi_n^{IV}(x) \Phi_m(x) dx = 0$$

Since the mode shapes are orthogonal, we simplify to:

$$\mu \ddot{\eta}_n(t) \int_0^L \Phi_n^2(x) dx + EI \eta_n(t) \int_0^L \Phi_n^{IV}(x) \Phi_n(x) dx = 0$$

Considering that the eigenfunction are (6):

$$\begin{cases} \Phi_n(x) = \sin\left(\frac{n\pi x}{L}\right) \\ \Phi_n^{IV}(x) = \left(\frac{n\pi}{L}\right)^4 \sin\left(\frac{n\pi x}{L}\right) \end{cases}$$

And the integral solutions:

$$\begin{cases} \int_0^L \Phi_n^2(x) dx = \int_0^L \sin^2\left(\frac{n\pi x}{L}\right) dx = \frac{L}{2} \\ \int_0^L \Phi_n^{IV}(x) \Phi_n(x) dx = \int_0^L \left(\frac{n\pi}{L}\right)^4 \sin^2\left(\frac{n\pi x}{L}\right) dx = \frac{L}{2} \left(\frac{n\pi}{L}\right)^4 \end{cases}$$

Substitute in the general equation and get:

$$\frac{L}{2} \mu \ddot{\eta}_n + \frac{L}{2} \left(\frac{n\pi}{L}\right)^4 EI \eta_n = 0$$

## Appendix D – Conductor self-damping term

The damping term developed by Diana needs to be studied with the Lagrangian approach. Considering a segment of cable [7], the kinetic and potential partial energy are:

$$\begin{cases} dT = \frac{1}{2} \mu \dot{w}^2 dx \\ dV = \frac{1}{2} EI \left( \frac{\partial^2 w}{\partial x^2} \right)^2 dx + \frac{1}{2} S \left( \frac{\partial w}{\partial x} \right)^2 dx \end{cases}$$

Remembering that  $w_n(x, t) = \eta_n(t) \Phi_n(x)$        $\Phi_n(x) = \sin\left(\frac{n\pi x}{L}\right)$

$$w(x, t) \approx \sum_{n=1}^N \eta_n(t) \Phi_n(x)$$

Substituting and integrating over the spatial domain:

$$\begin{cases} T_n = \frac{1}{2} \mu \dot{\eta}_n^2 \int_0^L \Phi_n^2 dx \\ V_n = \frac{1}{2} EI \eta_n^2 \int_0^L \left( \frac{\partial^2 \Phi_n}{\partial x^2} \right)^2 dx + \frac{1}{2} S \eta_n^2 \int_0^L \left( \frac{\partial \Phi_n}{\partial x} \right)^2 dx \end{cases}$$

Where :

$$\begin{cases} \int_0^L \Phi_n^2 dx = \frac{L}{2} \\ \int_0^L \left( \frac{\partial^2 \Phi_n}{\partial x^2} \right)^2 dx = \frac{n^4 \pi^4}{2L^3} \\ \int_0^L \left( \frac{\partial \Phi_n}{\partial x} \right)^2 dx = \frac{n^2 \pi^2}{2L} \end{cases}$$

So we can write:

$$\begin{cases} T_n = \frac{\mu L}{4} \dot{\eta}_n^2 \\ V_n = \left[ \frac{n^2 \pi^2}{4L} \left( \frac{n^2 \pi^2}{L^2} EI + S \right) \right] \eta_n^2 \end{cases}$$

In matrix form:

$$\begin{cases} T = \frac{1}{2} \{\dot{\eta}\}^T [m] \{\dot{\eta}\} \\ V = \frac{1}{2} \{\eta\}^T [k] \{\eta\} \end{cases}$$

Where  $[m]$  is the modal mass matrix:  $[m] = \text{diag}(m_n)$  and  $m_n = \frac{\mu L}{2}$  is the modal mass equal for each node.

For the calculation of self-damping component, we consider a hysteretic force acting on the cable as:

$$F = h \frac{\dot{w}}{\Omega}$$

The energy dissipated by each mode of vibration is:

$$dD_n = \frac{1}{2} \frac{h_n}{\Omega} \dot{w}_n^2 dx$$

Following the same steps kinetic energy and potential component:

$$D_n = \frac{L}{4} \frac{h_n}{\Omega} \dot{\eta}_n^2$$

Having all terms needed in Lagrange equation:

$$\frac{d}{dt} \frac{\partial T_n}{\partial \dot{\eta}_n} - \frac{\partial V_n}{\partial \eta_n} + \frac{\partial D_n}{\partial \dot{\eta}_n} = Q_n$$

We finally can write:

$$\frac{\mu L}{2} \ddot{\eta}_n - \left[ \frac{n^2 \pi^2}{2L} \left( \frac{n^2 \pi^2}{L^2} EI + S \right) \right] \eta_n + \frac{L}{2} \frac{h_n}{\Omega} \dot{\eta}_n = Q_n$$

## Appendix E – Modal matrix calculation

Considering only first cable:

$$\mu \frac{\partial^2 w_A}{\partial t^2} + k \frac{\partial^4 w_A}{\partial x^4} - S \frac{\partial^2 w_A}{\partial x^2} + \left( m_{AB} \frac{\partial^2 w_A}{\partial t^2} + k_{AB}(w_A - w_B) \right) \sum_{h=1}^H \delta(x - x_h) = f(x, t)$$

$$w_A(x, t) = \{\Phi(x)\}^T \{\eta_A(t)\}$$

$$\{\Phi(x)\}_{N \times 1} = \begin{Bmatrix} \sin\left(\frac{\pi x}{L}\right) \\ \sin\left(\frac{2\pi x}{L}\right) \\ \vdots \\ \sin\left(\frac{N\pi x}{L}\right) \end{Bmatrix} \quad \{\eta_A(t)\}_{N \times 1}$$

Substitute  $w_A(x, t)$  in the equation:

$$\begin{aligned} \mu \{\Phi\}^T \{ \ddot{\eta} \} + k \{\Phi^{IV}\}^T \{ \eta \} - S \{\Phi^{II}\}^T \{ \eta \} \\ + [m_{AB} \{\Phi\}^T \{ \ddot{\eta} \} + k_{12} \{\Phi\}^T (\{ \eta \} - \{ \eta_B \})] \sum_{h=1}^H \delta(x - x_h) = f(x, t) \end{aligned}$$

Multiply by  $\{\Phi\}$  and integrate over spatial domain:

$$\begin{aligned} \mu \int_0^L \{\Phi\} \{\Phi\}^T \{ \ddot{\eta} \} dx + k \int_0^L \{\Phi\} \{\Phi^{IV}\}^T \{ \eta \} dx - S \int_0^L \{\Phi\} \{\Phi^{II}\}^T \{ \eta \} dx \\ + m_{AB} \int_0^L \{\Phi\} \{\Phi\}^T \{ \ddot{\eta} \} \sum_{h=1}^H \delta(x - x_h) dx \\ + k_{AB} \int_0^L \{\Phi\} \{\Phi\}^T (\{ \eta \} - \{ \eta_B \}) \sum_{h=1}^H \delta(x - x_h) dx = \int_0^L \{\Phi\} f(x, t) dx \end{aligned}$$

Where:

$$\begin{cases} \Phi_n = \sin\left(\frac{n\pi x}{L}\right) \\ \Phi_n^I = \left(\frac{n\pi}{L}\right) \cos\left(\frac{n\pi x}{L}\right) \\ \Phi_n^{II} = -\left(\frac{n\pi}{L}\right)^2 \sin\left(\frac{n\pi x}{L}\right) \\ \Phi_n^{III} = -\left(\frac{n\pi}{L}\right)^3 \cos\left(\frac{n\pi x}{L}\right) \\ \Phi_n^{IV} = \left(\frac{n\pi}{L}\right)^4 \sin\left(\frac{n\pi x}{L}\right) \end{cases}$$

The integral terms are examined in the following.

- First term:  $\mu \int_0^L \{\Phi\}\{\Phi\}^T dx \{A\ddot{\eta}\}$

$$\begin{aligned} \{\Phi\}\{\Phi\}^T &= \begin{pmatrix} \sin\left(\frac{\pi x}{L}\right) \\ \sin\left(\frac{2\pi x}{L}\right) \\ \vdots \\ \sin\left(\frac{N\pi x}{L}\right) \end{pmatrix} \left\{ \sin\left(\frac{\pi x}{L}\right) \quad \sin\left(\frac{2\pi x}{L}\right) \quad \dots \quad \sin\left(\frac{N\pi x}{L}\right) \right\} \\ &= \begin{pmatrix} \sin^2\left(\frac{\pi x}{L}\right) & \sin\left(\frac{\pi x}{L}\right)\sin\left(\frac{2\pi x}{L}\right) & \dots & \dots \\ \sin\left(\frac{\pi x}{L}\right)\sin\left(\frac{2\pi x}{L}\right) & \sin^2\left(\frac{2\pi x}{L}\right) & \dots & \dots \\ \vdots & \vdots & \ddots & \vdots \\ \dots & \dots & \dots & \sin^2\left(\frac{N\pi x}{L}\right) \end{pmatrix}_{N \times N} \end{aligned}$$

The result of the integral is:

$$\int_0^L \sin^2\left(\frac{n\pi x}{L}\right) dx = \frac{L}{2} \quad \text{and} \quad \int_0^L \sin\left(\frac{k\pi x}{L}\right)\sin\left(\frac{m\pi x}{L}\right) dx = 0, \quad k \neq m$$

So, we get a diagonal matrix and can write the entire member as:

$$\mu_A \frac{L}{2} [I]_{N \times N} \{A\ddot{\eta}\}$$

Where  $[I]$  is the identity matrix.

- For second and third member we apply the same demonstration and get:

$$\begin{aligned} k \int_0^L \{\Phi\}\{\Phi^{IV}\}^T dx &= k \frac{L}{2} \text{diag} \begin{pmatrix} \left(\frac{\pi}{L}\right)^4 \\ \left(\frac{2\pi}{L}\right)^4 \\ \vdots \\ \left(\frac{N\pi}{L}\right)^4 \end{pmatrix}_{N \times N} \\ -S \int_0^L \{\Phi\}\{\Phi^{II}\}^T dx &= S \frac{L}{2} \text{diag} \begin{pmatrix} \left(\frac{\pi}{L}\right)^2 \\ \left(\frac{2\pi}{L}\right)^2 \\ \vdots \\ \left(\frac{N\pi}{L}\right)^2 \end{pmatrix}_{N \times N} \end{aligned}$$

- Fourth term:  $m_{AB} \int_0^L \{\Phi\}\{\Phi\}^T \sum_{h=1}^H \delta(x - x_h) dx$

For Dirac property:

$$\sum_{h=1}^H \int_0^L \{\Phi\}\{\Phi\}^T \delta(x - x_h) dx = \sum_{h=1}^H \{\Phi(x_h)\}\{\Phi(x_h)\}^T = [\Sigma_h]_{N \times N}$$

We can therefore write the final equation:

$$\begin{aligned} \mu \frac{L}{2} [I] \{ {}_A \ddot{\eta}(t) \} + k \frac{L}{2} \text{diag} \left( \left( \frac{n\pi}{L} \right)^4 \right) \{ {}_A \eta(t) \} + S \frac{L}{2} \text{diag} \left( \left( \frac{n\pi}{L} \right)^2 \right) \{ {}_A \eta(t) \} \\ + m_{AB} [\Sigma_h] \{ {}_A \ddot{\eta}(t) \} + k_{AB} [\Sigma_h] (\{ {}_A \eta(t) \} - \{ {}_B \eta(t) \}) \\ = \int_0^L \{\Phi(x)\} f(x, t) dx \end{aligned}$$

## Appendix F – Modal matrix of the coupled system

The initial equation of motion is:

$$[M]\{\ddot{\eta}\} + [K]\{\eta\} = \{F\}$$

Where  $\{\eta(t)\}_{2N \times 1} = \begin{Bmatrix} \{A\eta\} \\ \{B\eta\} \end{Bmatrix}$

After the EVP ( $[M]\{\ddot{\eta}\} + [K]\{\eta\} = 0$ ) we get the following modal matrix:

$$[Z]_{2N \times 2N} = \begin{bmatrix} [AZ] \\ [BZ] \end{bmatrix} = \begin{bmatrix} AZ_{1,1} & AZ_{1,2} & \dots & AZ_{1,2N} \\ AZ_{2,1} & AZ_{2,2} & \dots & AZ_{2,2N} \\ \vdots & \vdots & \ddots & \vdots \\ AZ_{N,1} & AZ_{N,2} & \dots & AZ_{N,2N} \\ BZ_{1,1} & BZ_{1,2} & \dots & BZ_{1,2N} \\ BZ_{2,1} & BZ_{2,2} & \dots & BZ_{2,2N} \\ \vdots & \vdots & \ddots & \vdots \\ BZ_{N,1} & BZ_{N,2} & \dots & BZ_{N,2N} \end{bmatrix}$$

The natural frequencies of the coupled system can be stacked into a 2N vector as:

$$\{\omega\} = \begin{pmatrix} \omega_1 \\ \omega_2 \\ \vdots \\ \omega_{2N} \end{pmatrix}$$

We can write:  $\{\eta(t)\} = [Z]\{p(t)\}$  where  $\{p(t)\}_{2N \times 1} = \begin{pmatrix} p_1 \\ p_2 \\ \vdots \\ p_{2N} \end{pmatrix}$

After substituting  $\{\eta(t)\}$  and pre-multiplying by  $[Z]^T$  we get:

$$[Z]^T[M][Z]\{\ddot{p}\} + [Z]^T[K][Z]\{p\} = [Z]^T\{F\}$$

$$\{F\}_{2N \times 1} = \begin{Bmatrix} \{A^F\} \\ \{B^F\} \end{Bmatrix}$$

If a distributed force is acting only on the first cable (A), we get:

$$\begin{aligned} \{F\}_{2N \times 1} &= \begin{Bmatrix} \{A^F\} \\ \{0\} \end{Bmatrix} = \begin{Bmatrix} \left\{ \int_0^L f \Phi_n dx \right\}_{N \times 1} \\ \{0\} \end{Bmatrix} = \begin{Bmatrix} \left\{ F_c \frac{L(1 - \cos(n\pi))}{n\pi} \sin(\Omega t) \right\}_{N \times 1} \\ \{0\} \end{Bmatrix} \\ &= \begin{Bmatrix} \begin{pmatrix} A^F_1 \\ A^F_2 \\ \vdots \\ A^F_N \end{pmatrix} \\ \{0\} \end{Bmatrix} \end{aligned}$$

Where  $F_c$  is the lift force of the wind and  $\Omega$  is the angular frequency of the wind.

In terms of modal force, it yields:

$$\begin{aligned} [Z]^T \{F\} &= \begin{bmatrix} AZ_{1,1} & AZ_{2,1} & \dots & AZ_{N,1} & BZ_{1,1} & BZ_{2,1} & \dots & BZ_{N,1} \\ AZ_{1,2} & AZ_{2,2} & \dots & AZ_{N,2} & BZ_{1,2} & BZ_{2,2} & \dots & BZ_{N,2} \\ \vdots & \vdots & & \vdots & \vdots & \vdots & & \vdots \\ AZ_{1,2N} & AZ_{2,2N} & \dots & AZ_{N,2N} & BZ_{1,2N} & BZ_{2,2N} & \dots & BZ_{N,2N} \end{bmatrix} \begin{Bmatrix} \begin{pmatrix} A^F_1 \\ A^F_2 \\ \vdots \\ A^F_N \end{pmatrix} \\ \{0\} \end{Bmatrix} \\ &= \begin{Bmatrix} \sum_{r=1}^N AZ_{r,1} A^F_r \\ \sum_{r=1}^N AZ_{r,2} A^F_r \\ \vdots \\ \sum_{r=1}^N AZ_{r,2N} A^F_r \end{Bmatrix}_{2N \times 1} = \begin{Bmatrix} \sum_{r=1}^N AZ_{r,1} F_c \frac{L(1 - \cos(r\pi))}{r\pi} \sin(\Omega t) \\ \sum_{r=1}^N AZ_{r,2} F_c \frac{L(1 - \cos(r\pi))}{r\pi} \sin(\Omega t) \\ \vdots \\ \sum_{r=1}^N AZ_{r,2N} F_c \frac{L(1 - \cos(r\pi))}{r\pi} \sin(\Omega t) \end{Bmatrix} \end{aligned}$$

Thus, the forced problem can be written as:

$$[Z]^T [M] [Z] \{\ddot{p}\} + [Z]^T [K] [Z] \{p\} = [Z]^T \{F\}$$

All the matrices are diagonal, so we can write the equation for each mode. As  $\{m_n\} = \text{diag}([Z]^T [M] [Z])$ :

$$\ddot{p}_n + \omega_n^2 p_n = \frac{F_c}{m_n} \sum_{r=1}^N AZ_{r,n} \frac{L(1 - \cos(r\pi))}{r\pi} \sin(\Omega t)$$

The solution can be obtained by employing the convolution integral:

$$\begin{aligned} \ddot{p}_n + \omega_n^2 p_n &= Q_n(t) \\ p_n(t) &= \int_0^t \frac{1}{\omega_n} Q_n(\tau) \sin \omega_n(t - \tau) d\tau \end{aligned}$$

Eventually, we can write:

$$p_n(t) = \frac{F_c}{m_n} \left[ \sum_{r=1}^N A Z_{r,n} \frac{L(1 - \cos(r\pi))}{r\pi} \right] \frac{1}{\omega_n^2 - \Omega^2} (\sin\Omega t - \frac{\Omega}{\omega_n} \sin\omega_n t)$$

And:

$$\{\eta(t)\} = [Z]\{p(t)\} = \begin{bmatrix} [AZ] \\ [BZ] \end{bmatrix} \{p(t)\} = \begin{bmatrix} AZ_{1,1} & AZ_{1,2} & \dots & AZ_{1,2N} \\ AZ_{2,1} & AZ_{2,2} & \dots & AZ_{2,2N} \\ \vdots & \vdots & \ddots & \vdots \\ AZ_{N,1} & AZ_{N,2} & \dots & AZ_{N,2N} \\ BZ_{1,1} & BZ_{1,2} & \dots & BZ_{1,2N} \\ BZ_{2,1} & BZ_{2,2} & \dots & BZ_{2,2N} \\ \vdots & \vdots & \ddots & \vdots \\ BZ_{N,1} & BZ_{N,2} & \dots & BZ_{N,2N} \end{bmatrix} \begin{Bmatrix} p_1 \\ p_2 \\ \vdots \\ p_{2N} \end{Bmatrix}$$

$$= \begin{Bmatrix} \left( \sum_n^{2N} AZ_{1,n} p_n \right) \\ \left( \sum_n^{2N} AZ_{2,n} p_n \right) \\ \vdots \\ \left( \sum_n^{2N} AZ_{N,n} p_n \right) \\ \left( \sum_n^{2N} BZ_{1,n} p_n \right) \\ \left( \sum_n^{2N} BZ_{2,n} p_n \right) \\ \vdots \\ \left( \sum_n^{2N} BZ_{N,n} p_n \right) \end{Bmatrix} = \begin{Bmatrix} \{A\eta\} \\ \{B\eta\} \end{Bmatrix}$$

Remembering that:  ${}_A w(x, t) = \{\Phi(x)\}^T \{A\eta(t)\}$

$$\{\Phi(x)\}_{Nx1} = \begin{Bmatrix} \sin\left(\frac{\pi x}{L}\right) \\ \sin\left(\frac{2\pi x}{L}\right) \\ \vdots \\ \sin\left(\frac{N\pi x}{L}\right) \end{Bmatrix}$$

$${}_A W(x, t) = \left\{ \sin\left(\frac{\pi x}{L}\right) \quad \sin\left(\frac{2\pi x}{L}\right) \quad \dots \quad \sin\left(\frac{N\pi x}{L}\right) \right\} \left\{ \begin{array}{c} \sum_{n=1}^{2N} {}_A Z_{1,n} p_n \\ \sum_{n=1}^{2N} {}_A Z_{2,n} p_n \\ \vdots \\ \sum_{n=1}^{2N} {}_A Z_{N,n} p_n \end{array} \right\}$$

$$\begin{aligned} {}_A W(x, t) &= \sum_{k=1}^N \sin\left(\frac{k\pi x}{L}\right) \sum_{n=1}^{2N} {}_A Z_{k,n} p_n \\ &= \sum_{k=1}^N \sin\left(\frac{k\pi x}{L}\right) \left[ \sum_{n=1}^{2N} {}_A Z_{k,n} \frac{F_c}{m_n} \left( \sum_{r=1}^N {}_A Z_{r,n} \frac{L(1 - \cos(r\pi))}{r\pi} \right) \frac{1}{\omega_n^2 - \Omega^2} (\sin\Omega t - \frac{\Omega}{\omega_n} \sin\omega_n t) \right] \end{aligned}$$

$$\left\{ \begin{array}{l} {}_A W(x, t) = \sum_{k=1}^N \sin\left(\frac{k\pi x}{L}\right) \left[ \sum_{n=1}^{2N} {}_A Z_{k,n} \frac{F_c}{m_n} \left( \sum_{r=1}^N {}_A Z_{r,n} \frac{L(1 - \cos(r\pi))}{r\pi} \right) \frac{1}{\omega_n^2 - \Omega^2} (\sin\Omega t - \frac{\Omega}{\omega_n} \sin\omega_n t) \right] \\ {}_B W(x, t) = \sum_{k=1}^N \sin\left(\frac{k\pi x}{L}\right) \left[ \sum_{n=1}^{2N} {}_B Z_{k,n} \frac{F_c}{m_n} \left( \sum_{r=1}^N {}_A Z_{r,n} \frac{L(1 - \cos(r\pi))}{r\pi} \right) \frac{1}{\omega_n^2 - \Omega^2} (\sin\Omega t - \frac{\Omega}{\omega_n} \sin\omega_n t) \right] \end{array} \right\}$$

Considering the same distributed force acting on both cables:

$$\begin{aligned} \{ {}_A F \} &= \{ {}_B F \} = \left\{ F_c \frac{L(1 - \cos(n\pi))}{n\pi} \sin(\Omega t) \right\}_{N \times 1} \\ \{ F \}_{2N \times 1} &= \left\{ \left\{ \begin{array}{c} \int_0^L f \Phi_n dx \\ \int_0^L f \Phi_n dx \end{array} \right\}_{N \times 1} \right\} = \left\{ \left\{ \begin{array}{c} F_c \frac{L(1 - \cos(n\pi))}{n\pi} \sin(\Omega t) \\ F_c \frac{L(1 - \cos(n\pi))}{n\pi} \sin(\Omega t) \end{array} \right\}_{N \times 1} \right\} \\ &= \left\{ \left\{ \begin{array}{c} {}_A F_1 \\ {}_A F_2 \\ \vdots \\ {}_A F_N \\ {}_B F_1 \\ {}_B F_2 \\ \vdots \\ {}_B F_N \end{array} \right\} \right\} \end{aligned}$$

$$[Z]^T \{F\} = \begin{bmatrix} {}_A Z_{1,1} & {}_A Z_{2,1} & \dots & {}_A Z_{N,1} & {}_B Z_{1,1} & {}_B Z_{2,1} & \dots & {}_B Z_{N,1} \\ {}_A Z_{1,2} & {}_A Z_{2,2} & \dots & {}_A Z_{N,2} & {}_B Z_{1,2} & {}_B Z_{2,2} & \dots & {}_B Z_{N,2} \\ \vdots & \vdots & & \vdots & \vdots & \vdots & & \vdots \\ {}_A Z_{1,2N} & {}_A Z_{2,2N} & \dots & {}_A Z_{N,2N} & {}_B Z_{1,2N} & {}_B Z_{2,2N} & \dots & {}_B Z_{N,2N} \end{bmatrix} \begin{Bmatrix} \left( \begin{matrix} {}_A F_1 \\ {}_A F_2 \\ \vdots \\ {}_A F_N \end{matrix} \right) \\ \left( \begin{matrix} {}_B F_1 \\ {}_B F_2 \\ \vdots \\ {}_B F_N \end{matrix} \right) \end{Bmatrix}$$

$$= \begin{Bmatrix} \left( \sum_{r=1}^N {}_A Z_{r,1} {}_A F_r + \sum_{r=1}^N {}_B Z_{r,1} {}_B F_r \right) \\ \left( \sum_{r=1}^N {}_A Z_{r,2} {}_A F_r + \sum_{r=1}^N {}_B Z_{r,2} {}_B F_r \right) \\ \vdots \\ \left( \sum_{r=1}^N {}_A Z_{r,2N} {}_A F_r + \sum_{r=1}^N {}_B Z_{r,2N} {}_B F_r \right) \end{Bmatrix}_{2N \times 1}$$

$$= \begin{Bmatrix} \left( \sum_{r=1}^N ({}_A Z_{r,1} + {}_B Z_{r,1}) F_c \frac{L(1 - \cos(r\pi))}{r\pi} \sin(\Omega t) \right) \\ \left( \sum_{r=1}^N ({}_A Z_{r,2} + {}_B Z_{r,2}) F_c \frac{L(1 - \cos(r\pi))}{r\pi} \sin(\Omega t) \right) \\ \vdots \\ \left( \sum_{r=1}^N ({}_A Z_{r,2N} + {}_B Z_{r,2N}) F_c \frac{L(1 - \cos(r\pi))}{r\pi} \sin(\Omega t) \right) \end{Bmatrix}$$

Returning to:  $[Z]^T [M] [Z] \{\ddot{p}\} + [Z]^T [K] [Z] \{p\} = [Z]^T \{F\}$

$$\ddot{p}_n + \omega_n^2 p_n = \frac{F_c}{m_n} \sum_{r=1}^N ({}_A Z_{r,n} + {}_B Z_{r,n}) \frac{L(1 - \cos(r\pi))}{r\pi} \sin(\Omega t)$$

The solution can be obtained by employing the convolution integral:

$$\ddot{p}_n + \omega_n^2 p_n = Q_n(t)$$

$$p_n(t) = \int_0^t \frac{1}{\omega_n} Q_n(\tau) \sin \omega_n(t - \tau) d\tau$$

I finally write:

$$p_n(t) = \frac{F_c}{m_n} \left[ \sum_{r=1}^N ({}_A Z_{r,n} + {}_B Z_{r,n}) \frac{L(1 - \cos(r\pi))}{r\pi} \right] \frac{1}{\omega_n^2 - \Omega^2} \left( \sin \Omega t - \frac{\Omega}{\omega_n} \sin \omega_n t \right)$$

And:

$$\{\eta(t)\} = [Z]\{p(t)\} = \begin{bmatrix} \begin{matrix} AZ_{1,1} & AZ_{1,2} & \dots & AZ_{1,2N} \\ AZ_{2,1} & AZ_{2,2} & \dots & AZ_{2,2N} \\ \vdots & \vdots & \ddots & \vdots \\ AZ_{N,1} & AZ_{N,2} & \dots & AZ_{N,2N} \end{matrix} \\ \begin{matrix} BZ_{1,1} & BZ_{1,2} & \dots & BZ_{1,2N} \\ BZ_{2,1} & BZ_{2,2} & \dots & BZ_{2,2N} \\ \vdots & \vdots & \ddots & \vdots \\ BZ_{N,1} & BZ_{N,2} & \dots & BZ_{N,2N} \end{matrix} \end{bmatrix} \begin{Bmatrix} p_1 \\ p_2 \\ \vdots \\ p_{2N} \end{Bmatrix} = \begin{Bmatrix} \sum_{n=1}^{2N} AZ_{1,n}p_n \\ \sum_{n=1}^{2N} AZ_{2,n}p_n \\ \vdots \\ \sum_{n=1}^{2N} AZ_{N,n}p_n \\ \sum_{n=1}^{2N} BZ_{1,n}p_n \\ \sum_{n=1}^{2N} BZ_{2,n}p_n \\ \vdots \\ \sum_{n=1}^{2N} BZ_{N,n}p_n \end{Bmatrix} = \begin{Bmatrix} \{A\eta\} \\ \{B\eta\} \end{Bmatrix}$$

Remembering that:  ${}_A W(x, t) = \{\Phi(x)\}^T \{A\eta(t)\}$

$$\{\Phi(x)\}_{Nx1} = \begin{Bmatrix} \sin\left(\frac{\pi x}{L}\right) \\ \sin\left(\frac{2\pi x}{L}\right) \\ \vdots \\ \sin\left(\frac{N\pi x}{L}\right) \end{Bmatrix}$$

$${}_A W(x, t) = \left\{ \sin\left(\frac{\pi x}{L}\right) \quad \sin\left(\frac{2\pi x}{L}\right) \quad \dots \quad \sin\left(\frac{N\pi x}{L}\right) \right\} \begin{Bmatrix} \sum_{n=1}^{2N} AZ_{1,n}p_n \\ \sum_{n=1}^{2N} AZ_{2,n}p_n \\ \vdots \\ \sum_{n=1}^{2N} AZ_{N,n}p_n \end{Bmatrix}$$

$$\begin{aligned} {}_A W(x, t) &= \sum_{k=1}^N \sin\left(\frac{k\pi x}{L}\right) \sum_{n=1}^{2N} AZ_{k,n}p_n \\ &= \sum_{k=1}^N \sin\left(\frac{k\pi x}{L}\right) \left[ \sum_{n=1}^{2N} AZ_{k,n} \frac{F_c}{m_n} \left( \sum_{r=1}^N ({}_A Z_{r,n} + {}_B Z_{r,n}) \frac{L(1 - \cos(r\pi))}{r\pi} \right) \frac{1}{\omega_n^2 - \Omega^2} (\sin\Omega t - \frac{\Omega}{\omega_n} \sin\omega_n t) \right] \end{aligned}$$

$$\begin{cases} {}_A W(x, t) = \sum_{k=1}^N \sin\left(\frac{k\pi x}{L}\right) \left[ \sum_{n=1}^{2N} AZ_{k,n} \frac{F_c}{m_n} \left( \sum_{r=1}^N ({}_A Z_{r,n} + {}_B Z_{r,n}) \frac{L(1 - \cos(r\pi))}{r\pi} \right) \frac{1}{\omega_n^2 - \Omega^2} (\sin\Omega t - \frac{\Omega}{\omega_n} \sin\omega_n t) \right] \\ {}_B W(x, t) = \sum_{k=1}^N \sin\left(\frac{k\pi x}{L}\right) \left[ \sum_{n=1}^{2N} BZ_{k,n} \frac{F_c}{m_n} \left( \sum_{r=1}^N ({}_A Z_{r,n} + {}_B Z_{r,n}) \frac{L(1 - \cos(r\pi))}{r\pi} \right) \frac{1}{\omega_n^2 - \Omega^2} (\sin\Omega t - \frac{\Omega}{\omega_n} \sin\omega_n t) \right] \end{cases}$$

If different external forces on the second cable, we'll have also different angular velocity  $\Omega$ .

$$\{F\}_{2N \times 1} = \left\{ \begin{array}{l} \left\{ \int_0^L f \Phi_n dx \right\}_{N \times 1} \\ \left\{ \int_0^L f \Phi_n dx \right\}_{N \times 1} \end{array} \right\} = \left\{ \begin{array}{l} \left\{ {}_A F_c \frac{L(1 - \cos(n\pi))}{n\pi} \sin({}_A \Omega t) \right\}_{N \times 1} \\ \left\{ {}_B F_c \frac{L(1 - \cos(n\pi))}{n\pi} \sin({}_B \Omega t) \right\}_{N \times 1} \end{array} \right\}$$

$$\ddot{p}_n + \omega_n^2 p_n = \frac{1}{m_n} \left[ \sum_{r=1}^N {}_A Z_{r,n} {}_A F_c \frac{L(1 - \cos(r\pi))}{r\pi} \sin({}_A \Omega t) + \sum_{r=1}^N {}_B Z_{r,n} {}_B F_c \frac{L(1 - \cos(r\pi))}{r\pi} \sin({}_B \Omega t) \right]$$

$$p_n(t) = \frac{1}{m_n} \left[ \sum_{r=1}^N {}_A Z_{r,n} {}_A F_c \frac{L(1 - \cos(r\pi))}{r\pi} \sin({}_A \Omega t) + \sum_{r=1}^N {}_B Z_{r,n} {}_B F_c \frac{L(1 - \cos(r\pi))}{r\pi} \sin({}_B \Omega t) \right] \frac{1}{\omega_{dn}^2 - \Omega^2} (\sin \Omega t - \frac{\Omega}{\omega_n} \sin \omega_n t)$$

And we reach the final equations:

$$\begin{cases} {}_A W(x, t) = \sum_{k=1}^N \sin\left(\frac{k\pi x}{L}\right) \left[ \sum_{n=1}^{2N} {}_A Z_{k,n} \frac{1}{m_n} \left[ \sum_{r=1}^N {}_A Z_{r,n} {}_A F_c \frac{L(1 - \cos(r\pi))}{r\pi} \sin({}_A \Omega t) + \sum_{r=1}^N {}_B Z_{r,n} {}_B F_c \frac{L(1 - \cos(r\pi))}{r\pi} \sin({}_B \Omega t) \right] \frac{1}{\omega_n^2 - {}_A \Omega^2} (\sin {}_A \Omega t - \frac{\Omega}{\omega_n} \sin \omega_n t) \right] \\ {}_B W(x, t) = \sum_{k=1}^N \sin\left(\frac{k\pi x}{L}\right) \left[ \sum_{n=1}^{2N} {}_B Z_{k,n} \frac{1}{m_n} \left[ \sum_{r=1}^N {}_A Z_{r,n} {}_A F_c \frac{L(1 - \cos(r\pi))}{r\pi} \sin({}_A \Omega t) + \sum_{r=1}^N {}_B Z_{r,n} {}_B F_c \frac{L(1 - \cos(r\pi))}{r\pi} \sin({}_B \Omega t) \right] \frac{1}{\omega_n^2 - {}_B \Omega^2} (\sin {}_B \Omega t - \frac{\Omega}{\omega_n} \sin \omega_n t) \right] \end{cases}$$

## Bibliography

- [1] EPRI, Transmission Line Reference Book: Wind-Induced Conductor Motion, 2006.
- [2] C. Diana, “Mathematical Analysis of Transmission Line Vibration,” 1969.
- [3] Rao, Vibration of Continuous Systems, 2007.
- [4] S. Sorrentino, D. Anastasio, A. Fasana and S. Marchesiello, “Distributed parameter and finite element models for wave,” 2017.
- [5] Gazzola, “Modelling and assessment of aeolian vibrations of overhead transmission line conductors,” 2018.
- [6] L. Meirovitch, Fundamentals of Vibration, New Jersey, 1999.
- [7] R. Bishop and D. C. Johnson, The Mechanics of Vibration., Cambridge, England: Cambridge University Press,, 1960.
- [8] A. Fasana and S. Marchesiello, Meccanica delle vibrazioni, 2006.
- [9] T. Timoshenko, Strength of Materials, Part 1: Elementary Theory and Problems, 2002.
- [10] T. Timoshenko, Strength of Materials, Part 2: Advanced Theory and Problems, 2002.
- [11] N. Barbieri, . O . H. de Souza Junior and R. Barbieri, Dynamical analysis of transmission line cables., 2002.